Mon. Not. R. Astron. Soc. **328,** 762–782 (2001)

The detection of molecular gas in the central galaxies of cooling flow clusters

A. C. Edge★
Department of Physics, University of Durham, South Road, Durham DH1 3LE

Accepted 2001 July 2. Received 2001 June 19; in original form 2001 January 15

ABSTRACT

We present the detections of CO line emission in the central galaxy of 16 extreme cooling flow clusters using the IRAM 30-m and the JCMT 15-m telescopes. These detections of CO(1–0), CO(2–1), CO(3–2) and CO(4–3) are consistent with the presence of a substantial mass of warm molecular gas ($10^{9-11.5}\,M_{\odot}$) within 50-kpc radius of the central galaxy. We present limits on 13 other galaxies in similarly extreme cooling flow clusters. These results are consistent with the presence of a massive starburst in the central galaxy, which warms a population of cold gas clouds producing both optical and near-infrared emission lines and significant CO line emission. Curiously, our CO detections are restricted to the lower radio power central galaxies. These are the first detections of molecular gas in a cooling flow other than NGC 1275 in the Perseus cluster. As four of our targets have firm limits on their dust mass from SCUBA and the rest have crude limits from *IRAS*, we can calculate gas-to-dust ratios. Simple analysis indicates that the best secondary indicator of molecular gas is optical line luminosity. We review the implications of these results and the prospects for observations in the near future.

Key words: galaxies: active – cooling flows – galaxies: starburst – submillimetre – X-rays: galaxies: clusters.

1 INTRODUCTION

The existence of cooling flows and the ultimate fate of this cooling gas have been the subject of an extensive and strongly contested debate for several decades (see Fabian 1994). The gas in the cores of massive, relaxed clusters of galaxies can cool and recombine through X-ray emission, initiating a cooling flow (Fabian & Nulsen 1977; Cowie & Binney 1977). The resulting reservoir of cold gas has not been detected in molecular form, and so is inferred either to reside in a phase with $T_{\rm gas} \ll 100\,{\rm K}$ (Ferland, Fabian & Johnstone 1994) or to indicate that cooling flows deposit much less gas if at all (O'Dea et al. 1994; Braine et al. 1995; Voit & Donahue 1995). The only cooling flow known to contain molecular gas is that around NGC 1275 in Perseus (Gear et al. 1985; Lester et al. 1995; Bridges & Irwin 1998), although the interpretation in this source is complicated by the strongly varying nuclear component. Moreover, the presence of the molecular gas may be related to an apparently on-going merger in this system, which has been the subject of a long-running debate (Van den Bergh 1977; Hu et al. 1983; Pedlar et al. 1990; Holtzman et al. 1992; Norgaard-Nielsen et al. 1993).

Recent results from optical emission-line ratios (Hansen, Jorgensen & Norgaard-Nielsen 1995; Allen 1995), *Hubble Space Telescope* (*HST*) imaging (McNamara et al. 1996; Pinkney et al. 1996) and submillimetre dust emission (Edge et al. 1999) all indicate that dust is present in the cores of massive cooling flows. As dust is rarely seen in the Universe without some accompanying molecular gas, it is timely to return to the limits on molecular gas in the massive cooling flows selected from the *ROSAT* All Sky Survey (e.g. Zw 3146: Edge et al. 1994; RX J1347−11: Allen 1998). This field has been dominated by non-detections (Grabelsky & Ulmer 1990; McNamara & Jaffe 1992; O'Dea et al. 1994; Braine & Dupraz 1994; Fujita et al. 2000), but improvements in receiver technology, combined with an increased pool of extreme cooling flows selected from *ROSAT* samples, offer new opportunities. Cooling flows with mass deposition rates of $>100\,M_{\odot}\,{\rm yr}^{-1}$ will accumulate molecular gas masses of $>10^{11}\,M_{\odot}$ in just $10^{9}\,{\rm yr}$; such masses are now detectable out to $z = 0.3$. Selecting more distant cooling flows allows more of the cooled gas to fall in the telescope beam, and permits observation of lines at more favourable frequencies [i.e. CO(3–2) in the A-band of the James Clerk Maxwell Telescope for $z > 0.25$]. With these factors in mind, we obtained two shifts of James Clerk Maxwell Telescope (JCMT) observations to search for CO(3–2) in the three most distant, massive cooling flows known at the time.

Throughout we assume $\Omega_0 = 1$ and $H_0 = 50\,{\rm km\,s^{-1}\,Mpc^{-1}}$.

★E-mail: Alastair.Edge@durham.ac.uk

2 OBSERVATIONS

The initial observations presented in this paper were obtained on 1998 December 26 and 27 using the recently commissioned A3i receiver on the JCMT on Mauna Kea in good conditions ($\tau_{CSO} = 0.05$–0.12). Three targets were observed, Zw 3146 ($z = 0.2906$, Edge et al. 1994), RX J1347 − 11 ($z = 0.4503$, Schindler et al. 1995) and RX J1532+30 ($z = 0.3615$, Ebeling et al. 1998) to search for the CO(3–2) transition redshifted into the A-band (210–276 GHz), and the exposures are summarized in Table 1. This project benefits greatly from the significant improvement in the performance of A3i over the previous A2 receiver in the 260–276 GHz range. However, owing to the unexpectedly poor performance of the A3i receiver in the frequency range of 245–255 GHz, the observation of RX J1532+30 is much less sensitive than the other two (T_{sys} of 800 K as opposed to 280–340 K), hence the limit set on this system is much weaker. Standard spectra of IRC+10216 were taken and flux calibration was made with Mars.

These observations were augmented by additional A3i observations on 1999 March 12 and May 1–3 and 15 of Zw 3146 using a larger bandwidth and slightly lower central frequency to compensate for the $-150\,km\,s^{-1}$ shift seen in the December data. The March observations were taken in poorer conditions ($\tau_{CSO} > 0.15$ and low elevation) so do not achieve sufficient sensitivity to detect the line, but the May data are better and confirm the initial detection (Fig. 1). During the May observations, we also obtained service time to observe ^{12}CO in A1835 and Zw 7160 (both $z \approx 0.25$, Allen et al. 1992) and ^{13}CO in A1835. All these JCMT observations were made in beam-switching mode with a throw of 60 or 90 arcsec.

Given the detections of CO(3–2), our next step was to obtain CO(1–0) observations with the IRAM 30-m telescope. We were awarded time contingent on a detection of Zw 3146 in service time on 1999 May 7. These data recovered a line of similar width and redshift to the initial JCMT detection, so we were allocated a total of 68 h in 1999 August. The data from this campaign were taken in good conditions for daytime, summer observing (2–8 mm atmospheric water vapour) so rapid progress was made. The observations are summarized in Table 2. A further 86 h was awarded in 2000 April, during which the weather was more favourable (1–5 mm atmospheric water vapour), and those observations are summarized in Table 3. All the IRAM observations were made in beam-switching mode with a throw of 210 arcsec. For our strongest ^{12}CO(1–0) detection (A1068), we also obtained ^{13}CO(1–0) data which set a strong limit on the isotopic ratio. For marginal detections we obtained, where possible, further data shifted in frequency by 150–400 MHz to eliminate possible non-linear baseline effects. These data confirmed the detections in most cases *but not all*. They are discussed individually in Section 4.

3 ANALYSIS

The JCMT data were analysed using the standard Starlink reduction package SPECX. After merging the separate sections of the Digital Autocorrelation Spectrometer (DAS) spectra and removing a linear baseline from them (excluding the $800\,km\,s^{-1}$ around the line), the spectra were co-added and binned to 12.5 MHz, and Hanning smoothed. Figs 1–3 present the spectra for CO(3–2), CO(4–3) and ^{13}CO(3–2) for all our JCMT observations, and the results of line fits to these spectra are presented in Table 4.

Fortuitously our observations on December 27 were made in very dry and stable sky conditions which are rarely used for low-frequency observations. The observations during this shift were exceptionally stable in baseline shifts (rms of 0.7 mK compared with 5.7 mK on December 26). This stability results in spectra far superior to all those in other sessions where the water vapour level was substantially higher and/or the baseline stability poorer. Therefore we have treated these spectra individually and used data taken in other sessions for confirmation of these results.

The IRAM 30-m data were analysed using the CLASS package.

Table 1. Log of JCMT observations.

Cluster	Date	Instrument	Frequency (GHz)	Bandwidth (MHz)	Exposure (s)	Conditions (τ_{CSO})	T_{sys} (K)	Beamsize (arcsec)
^{12}CO(3–2)								
Zw 3146	26/12/98	A3i	267.934	1000	6000	0.08	354	18.0
RX J1347−11	26/12/98	A3i	238.434	1000	7800	0.08	346	20.9
RX J1532+30	26/12/98	A3i	253.982	1000	6600	0.08	825	19.0
Zw 3146	27/12/98	A3i	267.934	1000	7200	0.05	292	18.0
RX J1347−11	27/12/98	A3i	238.434	1000	6600	0.05	279	20.9
RX J1532+30	27/12/98	A3i	253.982	1000	6000	0.05	748	19.0
Zw 3146	12/03/99	A3i	268.140	1800	5400	0.18	450	18.0
Zw 3146	01/05/99	A3i	268.140	1800	5400	0.12	413	18.0
A1835	2–3/05/99	A3i	276.130	1800	5700	0.13	452	17.5
A1835	15/05/99	A3i	276.130	1800	1800	0.12	496	17.5
Zw 7160	15/05/99	A3i	274.920	1800	1800	0.12	542	17.6
Zw 7160	24/05/99	A3i	274.920	1800	2700	0.14	486	17.6
A1835	31/05/99	A3i	276.130	1800	6600	0.15	480	17.5
Zw 7160	02/06/99	A3i	274.920	1800	6000	0.20	577	17.6
Zw 7160	19/06/99	A3i	274.920	1800	3600	0.10	389	17.6
^{13}CO(3–2)								
A1835	14–15/07/99	A3i	263.980	1800	7200	0.06	317	18.3
^{12}CO(4–3)								
Zw 3146	28–29/01/00	B3	357.410	1800	10200	0.07	410	13.6
RX J1532+30	28–29/01/00	B3	338.488	1800	11400	0.05	310	14.3
Zw 7160	20/07/97	B3	366.600	900	4200	0.05	603	13.2

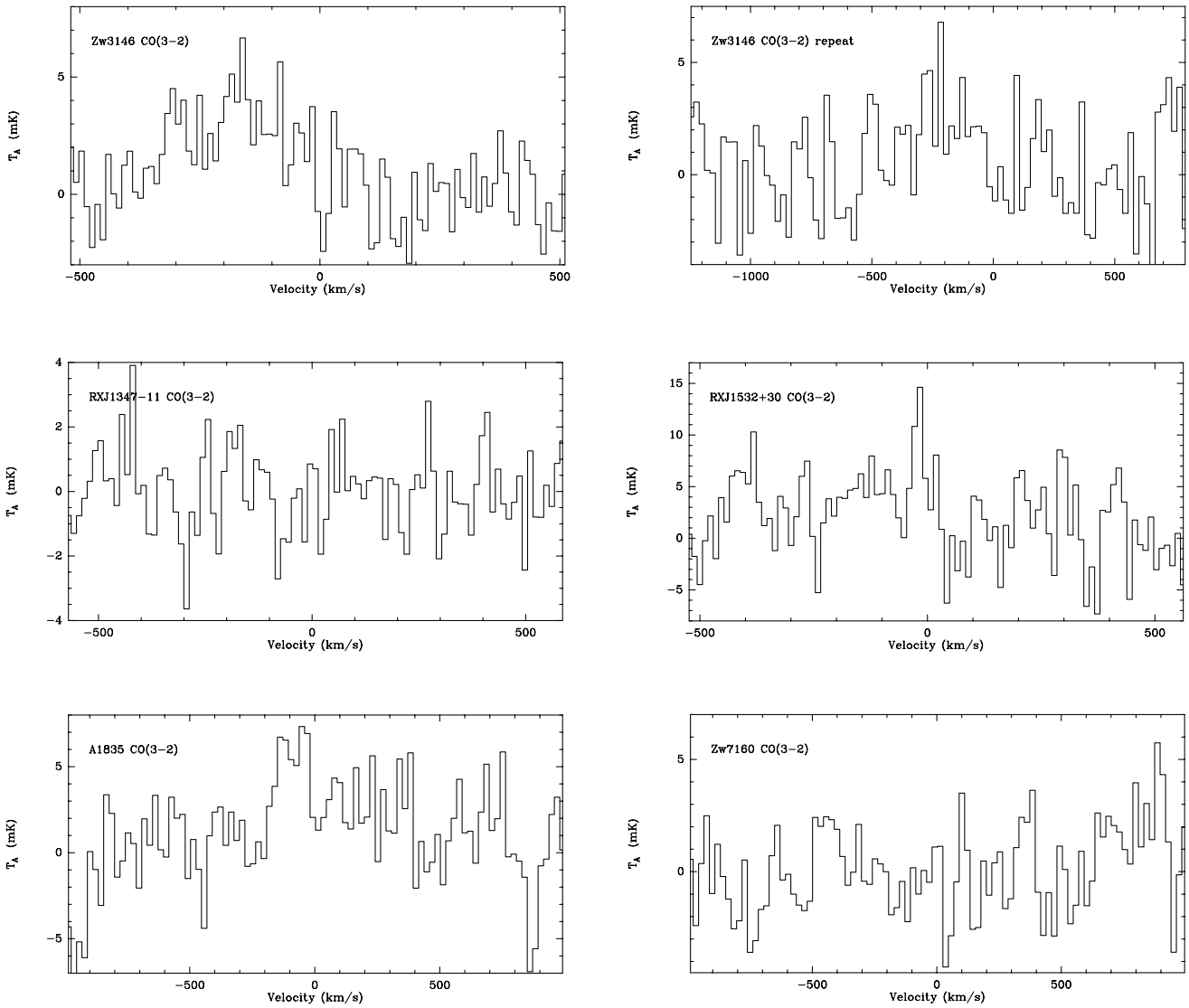

Figure 1. JCMT CO(3–2) spectra for Zw 3146, RX J1347−11, RX J1532+30, A1835 and Zw 7160.

The data were combined for both 500-MHz backends and both autocorrelators for the A100 and B100 receivers. The data had a linear baseline subtracted and were Hanning smoothed to 8-MHz resolution. Figs 4–8 present the CO(1–0) and CO(2–1) spectra for all our IRAM observations, and the results of the line fits to these spectra are presented in Tables 5 and 6.

The weather through both of the runs (largely daytime observations) was variable but only a few periods were poor (precipitable water above 8 mm), although 14 h were lost to high winds. Pointing observations were made every hour and temperature calibrations every 30 min. The pointing was always better than 5 arcsec throughout all observations.

Table 7 gives the continuum value where one is detected.

4 RESULTS

In this section we discuss the individual detections and limits for each source in order of first observation, and then present results for global properties of the molecular gas in these systems.

Zw 3146. This source has our most comprehensive data set and is confirmed at several different observed frequencies and for CO(1–0), CO(3–2) and CO(4–3). The line is relatively broad and slightly blueshifted compared with the optically determined velocity (Allen et al. 1992). This apparent blueshift may result (at least in part) from the intrinsic uncertainties in the optical spectra owing to their low resolution. However, there is a possibility that this velocity offset, and those observed in other galaxies, is related to the discrete nature of the molecular gas systems which are drawn from a broader velocity range (i.e. the cluster core dispersion of 400–800 km s^{-1}). Combining the JCMT and IRAM results, we derive a main-beam brightness temperature ratio for CO(3–2)/CO(1–0) of 0.83 ± 0.20 (correcting for the beamsize differences and beam efficiency), and for CO(4–3)/CO(3–2) of 0.89 ± 0.25. This is consistent with a temperature well in excess of 25 K.

RX J1347−11. This is the most distant cluster observed in this study, but also the most massive known cooling flow (Allen 1998). The high redshift precludes the observation of CO(1–0) with IRAM as it falls below the lowest tunable frequency of the A/B100 receivers. Our JCMT limit is particularly good thanks to the exceptionally favourable conditions under which the observations were made. There are several factors that may weaken this limit. The optical published spectroscopy for this galaxy is of low resolution (Schindler et al. 1995), so the true CO velocity may lie

Table 2. Log of IRAM observations from 1999.

Cluster	Date	Instrument	Frequency (GHz)	Bandwidth (MHz)	Exposure (s)	Conditions (mm H_2O)	T_{sys} (K)	Beamsize (arcsec)
^{12}CO(1–0)								
Zw 3146	6–7/05/99	A100	89.316	500	4920	4	125	26.9
A1068	31/07/99	A100	101.239	500	2640	4	137	23.8
A1835	31/07/99	A100	92.048	500	3840	4	130	26.1
Zw 3146	12/08/99	A100	89.316	500	3600	2	115	26.9
RX J1532+30	12/08/99	A100	84.665	500	3300	3	113	28.4
A2204	12/08/99	A100	100.114	500	3600	2	121	24.0
Zw 3916	13/08/99	A100	95.740	500	5640	7	141	25.1
Zw 8193	13/08/99	A100	97.448	500	6900	6	131	24.7
A2390	13/08/99	A100	93.542	500	6000	9	165	25.7
RX J0821+07	14/08/99	A100	103.848	500	3300	9	168	23.2
A2146	14/08/99	A100	93.390	500	5700	9	165	25.8
Zw 8193	14/08/99	A100	97.210	500	2400	7	136	24.7
Zw 7160	14/08/99	A100	91.645	500	6000	6	144	26.2
Zw 8197	14/08/99	A100	103.475	500	5400	3	128	23.2
RX J0352+19	15/08/99	A100	103.942	500	900	9	211	23.1
A646	15/08/99	A100	102.300	500	6120	8	154	23.5
A2204	15/08/99	A100	100.114	500	8400	9	148	24.0
A2390	15/08/99	A100	93.585	500	5220	7	147	25.7
A1068	16/08/99	A100	101.239	500	900	2	117	23.8
RX J1532+30	16/08/99	A100	84.600	500	4800	4	119	28.4
Zw 7160	16/08/99	A100	91.740	500	4950	2	132	26.2
Zw 8197	16/08/99	A100	103.540	500	5700	1	117	23.2
^{13}CO(1–0)								
A1068	01/08/99	A100	96.788	500	7680	5	124	24.8
^{12}CO(2–1)								
A1068	16/08/99	A230	202.487	500	900	2	301	11.9

outside the narrow bandwidth used. A velocity offset comparable to the largest that we observe in CO(1–0) between optical lines and CO could place the line outside the observed band. The only other published optical spectrum for the central galaxy is from Sahu et al. (1998) and shows strong Hα and [O I] 6300 Å. From their published spectrum we make a crude estimate of the Hα luminosity of $3 \pm 2 \times 10^{42}$ erg s^{-1}. Despite the non-detection of CO, the exceptional X-ray luminosity and mass flow rate of this cluster make it an important testbed for cooling flow predictions with future instrumentation (SOFIA, ALMA, *SIRTF*).

RX J1532+30. The operational difficulties with A3i during the JCMT observation of this galaxy prevent any firm conclusions being drawn from the CO(3–2) data alone, but when combined with our IRAM CO(1–0) and JCMT CO(4–3) data, a tentative CO(3–2) detection can be claimed. Our limits on CO(3–2)/CO(1–0) of 0.54 ± 0.18 and CO(4–3)/CO(3–2) of 0.77 ± 0.33 are consistent with other joint detections. This galaxy is our most massive molecular gas detection, and is the second most optically line-luminous central cluster galaxy in the Crawford et al. (1999) sample. This cluster has erroneously been claimed to be an active galaxy (Fischer et al. 1998), but *ROSAT* High Resolution Imager (HRI) imaging shows extended but strongly peaked emission consistent with a massive cooling flow (Crawford et al., in preparation).

A1835. The tuning range of A3i is just wide enough to obtain CO(3–2) for this cluster in the upper sideband. Both the JCMT and IRAM data show a consistent detection for this system. These data give a ratio of CO(3–2)/CO(1–0) of 0.47 ± 0.12 which is consistent with an excitation temperature of < 30 K. This is less than the temperature estimate from dust emission from Edge et al. (1999) of 40 ± 5 K. Given the observational scatter in all the observations, and the uncertainty of where the molecular emission lies in the JCMT beam, it would be premature to draw the conclusion that the gas in A1835 is significantly colder than the dust even if such differences are expected (Papadopoulos et al. 2000). However, the possibility that such low-temperature components are present is an exciting one. We also obtained a ^{13}CO(3–2) spectrum for A1835 (Fig. 3) which shows no significant emission. The data give a ^{12}CO/^{13}CO ratio of > 5 which rules out extremely optically thick clouds.

Zw 7160. The IRAM data for this cluster are quite ambiguous. Our first CO(1–0) observation shows a line at the $> 3\sigma$ level, which is also present in a subsequent, velocity-shifted observation in better conditions but with quite different line properties. Our JCMT data are not sensitive enough to detect the CO(3–2) line as most of the data were taken in comparatively poor conditions ($\tau_{CSO} > 0.12$). The ratio of CO(3–2)/CO(1–0) of < 0.55 is not restrictive. Our limit for CO(3–2) is consistent with that of Chapman et al. (2001) for CO(4–3) using B3 on JCMT. The CO(4–3) data have a restricted bandwidth and the line is placed close to the edge of the band, making a confirmation of the CO line impossible. Further JCMT B3 observations with a larger bandwidth would provide a significantly better limit. We claim a detection for this source, but wish to illustrate to the reader the difficulty in determining reliable line properties from such weak sources as we are working at the limits of single-dish capabilities.

A1068. This is our strongest detection and was significantly detected in the first 4 min of data. We observed ^{13}CO(1–0) and CO(2–1) for this system with IRAM. The former observation gives a firm limit on ^{12}CO/^{13}CO of > 10, indicating that the gas is not exceptionally optically thick and the isotopic ratio is comparable the value of 12 found in other galaxies (Young & Sanders 1986; Aalto et al. 1995; Papadopoulos & Seaquist 1998). If this limit applies to all other ^{12}CO detections then we predict that no ^{13}CO

Table 3. Log of IRAM observations from 2000. The exposures marked with an asterisk are those where only one receiver (A100) was available owing to a fault in B100.

Cluster	Date	Instrument	Frequency (GHz)	Bandwidth (MHz)	Exposure (s)	Conditions (mm H_2O)	T_{sys} (K)	Beamsize (arcsec)
^{12}CO(1–0)								
RX J0821+07	19/04/00	A100	103.760	500	1500	5	133	23.2
A1068	19/04/00	A100	101.245	1000	2100	5	107	23.8
A1664	19/04/00	A100	102.227	500	3600	5	160	23.5
A2390	20/04/00	A100	93.585	500	3600	3	113	25.7
A2597	20/04/00	A100	106.221	500	3900	4	138	22.6
RX J0352+19	20/04/00	A100	103.942	500	3600	3	132	23.1
RX J0439+05	20/04/00	A100	95.423	500	3600*	2	114	25.2
RX J0338+09	21/04/00	A100	111.502	500	2700*	2	148	21.6
RX J0338+09	21/04/00	A100	111.440	500	1800*	2	150	21.6
RX J0439+05	21/04/00	A100	93.580	500	4500	2	114	25.2
A2390	23/04/00	A100	93.635	500	2400	1	103	25.7
A2597	23/04/00	A100	106.150	500	3600	1	117	22.7
A262	23/04/00	A100	113.435	500	1800	1	148	21.2
RX J0338+09B	23/04/00	A100	111.440	500	1950	2	137	21.6
RX J0352+19	23/04/00	A100	104.000	500	1800	1	105	23.1
RX J0747−19	23/04/00	A100	104.054	500	3600	1	124	23.1
4C+55.16	23/04/00	A100	92.811	500	1800	1	104	25.9
4C+55.16	23/04/00	A100	92.717	500	2400	1	104	25.9
RX J0338+09B	24/04/00	A100	111.300	500	1800*	2	122	21.6
A262	24/04/00	A100	113.435	500	1800*	2	137	21.2
A478	24/04/00	A100	106.143	500	1800	1	109	22.7
RX J0747–19	24/04/00	A100	103.950	500	1800	2	124	23.1
Hydra A	24/04/00	A100	109.382	500	1500	2	137	22.0
A646	24/04/00	A100	102.240	500	3600	2	107	23.5
A2390	25/04/00	A100	93.750	500	2250	1	109	25.6
Zw 2089	16/06/00	A100	93.284	500	3900	7	130	25.7
A1664	16/06/00	A100	102.280	500	4320	5	139	23.5
Zw 2089	17/06/00	A100	93.284	500	4500	5	131	25.7
A1795	17/06/00	A100	108.419	500	4320	5	133	22.2
Zw 8276	25/07/00	A100	107.179	500	4050	6	136	22.4
A2390	25/07/00	A100	93.750	500	3600	7	117	25.6
A291	25/07/00	A100	96.381	500	4200	6	124	24.9
A11	02/08/00	A100	100.34	500	2850	12	182	24.0
A11	05/08/00	A100	100.25	500	3300	11	184	24.0
^{12}CO(2–1)								
RX J0821+07	19/04/00	A230	207.516	500	3600	5	352	11.6
A1068	19/04/00	A230	202.486	1000	2100	5	331	11.9
A2597	21/04/00	A230	212.336	1000	4800	2	306	11.3
RX J0352+19	23/04/00	A230	207.879	1000	1800	1	212	11.6
RX J0747−19	23/04/00	A230	208.104	1000	900	1	305	11.6
RX J0338+09B	24/04/00	A230	222.877	1000	1800	2	222	10.8
A262	24/04/00	A230	226.866	1000	1800	2	249	10.6
A478	24/04/00	A230	212.282	1000	1800	1	228	11.3

detections are possible with currently available instrumentation. The CO(2–1) data from 1999 August are likely to give an underestimate of the total line intensity owing to the narrow bandwidth used (500 km s^{-1}), but the 2000 April data were obtained with the 1-GHz backend and are much more reliable. The ratio of main-beam brightness temperatures for CO(2–1)/CO(1–0), correcting for beam size and efficiency, is 0.71 ± 0.08, so consistent *at face value* with a temperature of <30 K.

A2204. This is a relatively weak IRAM detection, which is clearer in the initial, shorter observation made in very good conditions but is present in the follow-up observation which was made in much poorer conditions. Unfortunately the second observation was made without a frequency shift, so our detection for this source not as secure as some of the other weak detections. That caveat aside, this system is one of the strongest optical line emitters within a redshift of 0.2, and lies in the second most massive cooling flow in the brightest 50 X-ray clusters (Peres et al. 1998), so is of particular importance for future studies.

Zw 3916. The IRAM data for this source give a good upper limit. There is weak excess at the low-velocity end of the spectrum, which could be a line offset from the optical velocity by >600 km s^{-1} which is strongly affected by the baseline subtraction, but there was not sufficient time to make a velocity-offset observation so this cannot be confirmed.

Zw 8193. This peculiar source is the most confused of the sample. The initial optical spectrum of the central galaxy gives significantly different redshifts for the stellar features and the emission lines (Allen et al. 1992). Recent *K*-band imaging and spectroscopy indicate that the most of the line emission comes from the region of a strong radio source offset by 2–3 arcsec from the bulk of the stellar continuum, and that this line emission shows a strong velocity shear. There is also a strong flat-spectrum radio source present that shows up in the IRAM data as a baseline of 3 mK (or 16 mJy), implying that the flat ($\alpha = -0.5$) spectrum continues to 100 GHz. This intrinsic complexity makes interpretation of the CO data non-trivial. The most that can be said from our

Table 4. Summary of JCMT results. All velocity shifts are quoted relative to the published optical redshift and are not relative to the observed frequency.

Cluster	Date	Line	Noise (mK)	Area (K km s^{-1})	Peak (mK)	Width (km s^{-1})	Velocity shift (km s^{-1})
Zw 3146	26/12/98	CO(3–2)	1.7	0.90 ± 0.33	3.2 ± 1.3	264 ± 120	-162 ± 103
	27/12/98	CO(3–2)	1.1	1.32 ± 0.23	4.3 ± 1.0	289 ± 89	-194 ± 45
	12/03/99	CO(3–2)	3.6	0.77 ± 0.36	2.4 ± 1.1	303 ± 120	-204 ± 93
	01/05/99	CO(3–2)	1.6	1.11 ± 0.28	3.2 ± 0.9	320 ± 95	-218 ± 52
	28–29/01/00	CO(4–3)	1.8	2.02 ± 0.33	5.5 ± 1.3	345 ± 90	-280 ± 44
RX J1347−11	26–27/12/98	CO(3–2)	0.7	<0.15	<0.5	300Fixed	−300−300
RX J1532+30	26–27/12/98	CO(3–2)	2.6	0.74 ± 0.25	4.3 ± 2.1	173 ± 103	-88 ± 35
	28–29/01/00	CO(4–3)	1.9	1.00 ± 0.20	2.3 ± 0.9	457 ± 103	-189 ± 35
A1835	2–3/05/99	CO(3–2)	2.2	0.77 ± 0.23	6.3 ± 2.3	129 ± 91	-108 ± 55
	15/05/99	CO(3–2)	3.7	0.98 ± 0.45	6.7 ± 2.9	149 ± 78	-119 ± 87
	31/05/99	CO(3–2)	1.7	1.03 ± 0.25	5.7 ± 2.2	168 ± 58	-77 ± 69
	14–15/07/99	^{13}CO(3–2)	1.3	<0.2	<1.2	168Fixed	−77Fixed
Zw 7160	all data	CO(3–2)	2.1	<0.25	<0.7	380Fixed	−233Fixed
	20/07/97	CO(4–3)	3.7	<1.42	<3.5	380Fixed	−233Fixed

data is that there is no strong, narrow (<300 km s^{-1}) component to the CO. Our first spectrum (the longer of the two) shows a very broad, flat-topped line. This line is consistent with two 300 km s^{-1} lines separated by 400 km s^{-1}. Our second spectrum shifts one of these lines to the edge of the spectrum, so the limits are poor as the line is weaker but the data are consistent within the errors. However, the complexity of the line prevents us claiming a CO detection in this system. Given the high optical line luminosity of this galaxy, the upper limit derived is of considerable importance (see Fig. 9, later) so this cooling flow demands further attention at all wavelengths.

A2390. Given the wealth of data on this cluster in the literature, we were keen to obtain CO data for it. We were somewhat surprised to find no detection of CO despite repeated, frequency-shifted observations, although the continuum level at 95 GHz is close to that expected from the radio/submillimetre spectrum of this galaxy in Edge et al. (1999). One possibility is that the CO emission has a very complex velocity structure. The presence of multiple velocity components in CO is not unexpected if the observed CO is related to discrete clouds such as are seen (or at least hinted at) in other distant galaxies (Papadopoulos et al. 2000). The *HST* image of the central galaxy in A2390 shows several 'blueknots' (Edge et al. 1999), so the two lines could be related to those. We note with interest the *HST* STIS spectrum of this galaxy presented by Hutchings & Balogh (2000) which shows a strong velocity gradient over the major axis of the central galaxy. The velocity shifts between the 'blue knots' are around 400–600 km s^{-1}, so we could be detecting CO associated with a number of star-forming regions, and no single narrow line is found. Given the spatial separation of the components in the STIS image (2 arcsec), it should be possible to resolve these two components spatially with current interferometers (Owens Valley, Plateau de Bure).

RX J0821+07. Despite being made during some of the worst conditions during the 1999 August run, the detection of this galaxy is clear. The line is the narrowest and the most offset in velocity from the optical value. The velocity offset is at least in part due to the rounding introduced by quoting redshifts to 3 decimal places by Crawford et al. (1995), but is largely due to the strong velocity shear found in the optical lines themselves (Wilman & Crawford, private communication). Significantly, this source is the third brightest *IRAS* source in this study so there is a broad trend for the more luminous far-infrared sources to be CO detections. Unfortunately the *IRAS* data are not deep or uniform enough to provide a definitive indicator.

A2146. The non-detection of this galaxy could be due to the presence of a strong active galactic nuclei (AGN) component to the ionization in this system (see Allen 1995). The X-ray emission around the galaxy is extended so it is more reminiscent of Cygnus A than of single, isolated AGN. The X-ray imaging and optical spectroscopy for this cluster indicate that it has significantly different properties from the majority of our other CO detections in that the galaxy is not at the centre of the cluster. The weak *IRAS* detection of the galaxy is consistent with either interpretation.

Zw 8197. This is one of our weakest CO detections, but it is reproduced in a frequency-shifted observation so we are confident of the detection. However, the absolute line intensity is sensitive to the baseline subtraction used, so the error on the intensity is large.

RX J0352+19. This source is detected in both CO(1–0) and CO(2–1), so we are confident of this detection despite the small integrated intensity.

A646. There is a very marginal detection of this galaxy in one of our two observations, so we do not claim this as a detection. The continuum detection in this source is consistent with a flat ($\alpha = -0.3$) source from 1 to 100 GHz.

A1664. This source is our most southerly target and was a challenging observation. We obtained a frequency-shifted confirmation of our 2000 April detection but could not obtain a CO(2–1) confirmation to put this detection beyond doubt.

A2597. This well-studied cooling flow has not been searched for CO until now. We made both CO(1–0) and CO(2–1) observations of A2597, and find a weak detection in our first observation that has a marginal CO(2–1) counterpart. The CO(1–0) detection is not confirmed in our frequency-shifted observation, but it was made in poorer conditions with the line close to the edge of the bandwidth. This is one of our least significant lines and needs much longer integrations of CO(2–1).

RX J0439+05. This central galaxy contains one of the strongest radio sources in the sample, although the 1.4-GHz flux density is relatively low because of the gigahertz-peaked nature of

Table 5. Summary of IRAM results for the 1999 data. The noise values are the rms in 8-MHz bins. Again all velocity shifts are quoted relative to the published optical redshift.

Cluster	Date	Line	Noise (mK)	Area (K km s^{-1})	Peak (mK)	Width (km s^{-1})	Velocity shift (km s^{-1})
Zw 3146	07/05/99	CO(1–0)	0.6	0.58 ± 0.09	1.5 ± 0.2	355 ± 69	-179 ± 25
	12/08/99	CO(1–0)	0.6	0.74 ± 0.13	1.7 ± 0.3	412 ± 92	-178 ± 39
A1068	31/07/99	CO(1–0)	1.0	1.82 ± 0.13	8.3 ± 0.6	207 ± 18	-16 ± 7
	01/08/99	^{13}CO(1–0)	0.5	<0.08	<0.4	207Fixed	−16Fixed
	16/08/99	CO(2–1)	3.6	3.73 ± 0.07	13.9 ± 0.3	251 ± 21	-42 ± 13
	16/08/99	CO(1–0)	1.6	2.60 ± 0.35	7.7 ± 1.0	319 ± 58	-20 ± 21
A1835	31/07/99	CO(1–0)	0.8	1.08 ± 0.13	4.5 ± 0.3	227 ± 38	-105 ± 12
RX J1532+30	12/08/99	CO(1–0)	0.7	0.34 ± 0.09	1.5 ± 0.6	217 ± 60	97 ± 30
	16/08/99	CO(1–0)	0.6	0.73 ± 0.11	1.4 ± 0.3	472 ± 85	-169 ± 37
A2204	12/08/99	CO(1–0)	0.9	0.41 ± 0.11	1.5 ± 0.3	255 ± 88	36 ± 31
	15/08/99	CO(1–0)	0.5	0.16 ± 0.05	0.9 ± 0.3	177 ± 42	-59 ± 28
Zw 3916	13/08/99	CO(1–0)	0.8	<0.15	<0.5	300Fixed	0Fixed
Zw 8193	13/08/99	CO(1–0)	0.6	0.51 ± 0.08	1.5 ± 0.3	313 ± 50	57 ± 23
				0.52 ± 0.07	1.8 ± 0.3	268 ± 35	460 ± 19
	14/08/99	CO(1–0)	1.2	0.72 ± 0.15	2.1 ± 0.7	313Fixed	57Fixed
				<0.20	<0.6	268Fixed	460Fixed
A2390	13/08/99	CO(1–0)	0.8	0.30 ± 0.08	1.4 ± 0.5	203 ± 61	-88 ± 30
				0.13 ± 0.08	1.9 ± 0.8	60 ± 38	-410 ± 11
	15/08/99	CO(1–0)	0.7	0.37 ± 0.08	1.5 ± 0.5	230 ± 48	-3 ± 24
				0.33 ± 0.07	1.7 ± 0.6	179 ± 50	-454 ± 22
RX J0821+07	14/08/99	CO(1–0)	1.1	1.30 ± 0.14	9.7 ± 1.0	126 ± 16	256 ± 6
A2146	14/08/99	CO(1–0)	0.8	0.15 ± 0.07	0.9 ± 0.5	168 ± 83	-416 ± 43
				0.14 ± 0.05	2.0 ± 0.5	67 ± 27	30 ± 11
Zw 7160	14/08/99	CO(1–0)	0.6	0.41 ± 0.09	1.0 ± 0.3	380 ± 77	-233 ± 43
Zw 7160	16/08/99	CO(1–0)	0.8	0.36 ± 0.14	0.6 ± 0.2	590 ± 189	-252 ± 58
Zw 8197	14/08/99	CO(1–0)	0.7	0.32 ± 0.07	1.3 ± 0.4	240 ± 55	-75 ± 276
Zw 8197	16/08/99	CO(1–0)	0.6	0.35 ± 0.08	1.0 ± 0.3	310 ± 68	-75 ± 15
RX J0352+19	15/08/99	CO(1–0)	2.4	<0.96	<1.5	300Fixed	0Fixed
A646	15/08/99	CO(1–0)	0.8	0.21 ± 0.11	0.9 ± 0.4	221 ± 97	125 ± 27

the nucleus. We detect the radio continuum at CO(1–0) and find no evidence for broad emission or narrow absorption lines.

RX J0338+09. The cluster was included in the study of Braine & Dupraz (1994) and a marginal line is visible in their figures. We observed this galaxy in two positions: on the cD and at a point 8 arcsec north-west of the cD where the Hα emission is strongest (Romanishin & Hintzen 1988). Both positions show evidence for a line but it is strongest offset from the cD. The detection is confirmed at CO(2–1) and has very recently been observed by the Owens Valley Radio Observatory (OVRO) so a clearer picture of the extent of the CO emission will follow soon.

A262. Like RX J0338+09, A262 is a cluster in which we contradict the non-detection of Braine & Dupraz (1994). The CO(1–0) and CO(2–1) detections give a relatively low ratio of C(2–1)/CO(1–0) of 0.25, but this may be due to the CO emission overfilling the CO(2–1) beam.

RX J0747−19 aka PKS 0745−191. This galaxy was observed on several occasions by us and has been studied in CO by O'Dea et al. (1994) with the Swedish–ESO Submillimetre Telescope (SEST). The smaller beamsize of the IRAM 30-m allows a significantly better limit to be set in this paper. We find no evidence for a narrow line (<500 km s^{-1}) but a wide line is possible. The weak continuum is consistent with the continuation of the steep radio spectrum.

A478. This classic cooling flow has not been studied in any great detail for CO, at least in part because of the poor redshift of the central galaxy in the literature for many years. Our CO(1–0) observation shows a marginal detection, but the CO(2–1) observation is more significant and makes us confident of this detection.

4C+55.16. This cluster has only recently been recognized as a strong cooling flow (Iwasawa et al. 1999), and contains a remarkably bright, flat-spectrum radio source. We clearly detect the continuum at CO(1–0) consistent with the 5–30 GHz spectral index of -1.3, but find no evidence for a line in emission or absorption. This source may provide one of the strongest constraints on CO in absorption given its strong, compact nucleus.

Hydra-A. This galaxy was observed once by us and has been studied in CO(2–1) by McNamara & Jaffe (1994). We find no evidence for a narrow line (<500 km s^{-1}), but a wide line is possible. The continuum level is consistent with the lower frequency radio data, but the published continuum level of 17 mK, or 267 mJy, at 218 GHz by McNamara & Jaffe (1994) implies that the

Table 6. Summary of IRAM results for the 2000 data. The noise values are the rms in 8-MHz bins.

Cluster	Date	Line	Noise (mK)	Area (K km s^{-1})	Peak (mK)	Width (km s^{-1})	Velocity shift (km s^{-1})
RX J0821+07	19/04/00	CO(1–0)	1.1	1.64 ± 0.12	8.1 ± 2.1	191 ± 17	260 ± 7
	19/04/00	CO(2–1)	3.1	2.90 ± 0.19	20.0 ± 3.0	137 ± 11	260 ± 5
A1068	19/04/00	CO(1–0)	1.2	1.75 ± 0.17	7.3 ± 2.0	226 ± 25	−6 ± 11
	19/04/00	CO(2–1)	4.0	5.74 ± 0.31	22.2 ± 3.0	243 ± 13	2 ± 6
A1664	19/04/00	CO(1–0)	1.3	1.86 ± 0.26	2.1 ± 1.0	823 ± 121	−52 ± 56
A1664	16/06/00	CO(1–0)	1.1	1.10 ± 0.18	1.7 ± 0.4	592 ± 99	−56 ± 76
A2390	20/04/00	CO(1–0)	0.7	<0.2	<0.6	300Fixed	−300–300
	23/04/00	CO(1–0)	1.0	<0.2	<1.0	300Fixed	−300–300
	25/04/00	CO(1–0)	1.0	<0.2	<1.0	300Fixed	−300–300
	25/07/00	CO(1–0)	0.9	<0.2	<0.9	300Fixed	−300–300
A2597	20/04/00	CO(1–0)	0.9	0.33 ± 0.11	1.1 ± 0.4	278 ± 88	108 ± 48
	21/04/00	CO(2–1)	2.6	0.47 ± 0.19	1.5 ± 0.6	300Fixed	130 ± 67
RX J0352+19	20/04/00	CO(1–0)	0.8	0.41 ± 0.11	1.1 ± 0.3	350 ± 76	21 ± 42
	23/04/00	CO(1–0)	1.1	0.53 ± 0.10	2.3 ± 1.0	213 ± 55	55 ± 19
	23/04/00	CO(2–1)	3.1	1.20 ± 0.24	3.7 ± 1.4	304 ± 65	−11 ± 31
RX J0439+05	20/04/00	CO(1–0)	1.0	<0.3	<1.0	300Fixed	−300–300
RX J0338+09	21/04/00	CO(1–0)	1.1	1.29 ± 0.14	3.2 ± 1.7	376 ± 40	176 ± 21
RX J0338+09B	23/04/00	CO(1–0)	0.8	1.45 ± 0.14	3.4 ± 1.0	402 ± 44	175 ± 21
	24/04/00	CO(1–0)	1.8	1.05 ± 0.25	3.8 ± 1.2	256 ± 62	170 ± 31
	24/04/00	CO(2–1)	3.6	2.83 ± 0.24	6.8 ± 1.1	391 ± 37	174 ± 86
A262	23/04/00	CO(1–0)	1.2	1.50 ± 0.22	3.1 ± 1.1	456 ± 75	13 ± 35
	24/04/00	CO(1–0)	1.2	1.68 ± 0.20	3.3 ± 1.0	473 ± 60	18 ± 27
	24/04/00	CO(2–1)	2.8	1.61 ± 0.26	4.1 ± 1.2	371 ± 67	29 ± 30
RX J0747–19	23/04/00	CO(1–0)	0.8	<0.30	<1.0	300Fixed	−300–300
	23/04/00	CO(2–1)	5.9	<1.0	<3.0	300Fixed	−300–300
	24/04/00	CO(1–0)	1.3	<0.30	<1.1	300Fixed	−300–300
4C +55.16	23/04/00	CO(1–0)	1.1	<0.30	<1.0	300Fixed	−300–300
A478	24/04/00	CO(1–0)	0.8	0.24 ± 0.14	1.0 ± 0.4	231 ± 62	−154 ± 53
	24/04/00	CO(2–1)	2.9	0.54 ± 0.17	4.4 ± 1.0	120 ± 16	−58 ± 18
Hydra A	24/04/00	CO(1–0)	1.3	<0.3	<1.1	300Fixed	−300–300
A646	24/04/00	CO(1–0)	0.6	<0.2	<0.5	300Fixed	−300–300
Zw 2089	16–17/06/00	CO(1–0)	0.5	0.11 ± 0.04	1.5 ± 1.0	67 ± 33	−197 ± 13
A1795	17/06/00	CO(1–0)	1.0	0.23 ± 0.06	2.1 ± 1.1	100 ± 33	−235 ± 15
Zw 8276	25/07/00	CO(1–0)	0.6	0.60 ± 0.09	1.3 ± 0.3	440 ± 62	−106 ± 34
A291	25/07/00	CO(1–0)	0.8	0.16 ± 0.08	0.7 ± 0.4	218 ± 93	254 ± 60
A11	02/08/00	CO(1–0)	1.1	0.46 ± 0.12	2.2 ± 1.1	191 ± 56	103 ± 24
				0.45 ± 0.13	2.2 ± 1.0	188 ± 72	535 ± 31
	05/08/00	CO(1–0)	0.9	0.45 ± 0.14	3.7 ± 1.5	114 ± 58	96 ± 13
				0.44 ± 0.14	2.0 ± 0.9	209 ± 88	676 ± 24

radio/submillimetre spectrum may flatten around 150 GHz. The continuum data imply that SCUBA would detect around 100 mJy at 850 μm.

Zw 2089. This cooling flow, although selected from the Brightest Cluster Sample (BCS; Ebeling et al. 1998), is not part of the Crawford et al. (1999) spectroscopic sample, but is a strong optical line emitter. Our observations show no strong line but do indicate a repeated narrow line. We do not claim any detection, but further CO observations may be justified in the future.

A1795. This galaxy was observed once by us and has been studied in CO by two groups (Ulmer & Grabelsky 1990; Braine & Dupraz 1994). We find a marginal line in a single service observation, but this claim requires a frequency-shifted reconfirmation and/or CO(2–1) observations before it can be regarded as secure. This galaxy has an unusual optical line emission filament (see Fabian et al. 2001b), so further CO observations are necessary to search for similarly extended molecular gas.

Zw 8276. Again, this galaxy has a detection in a single service

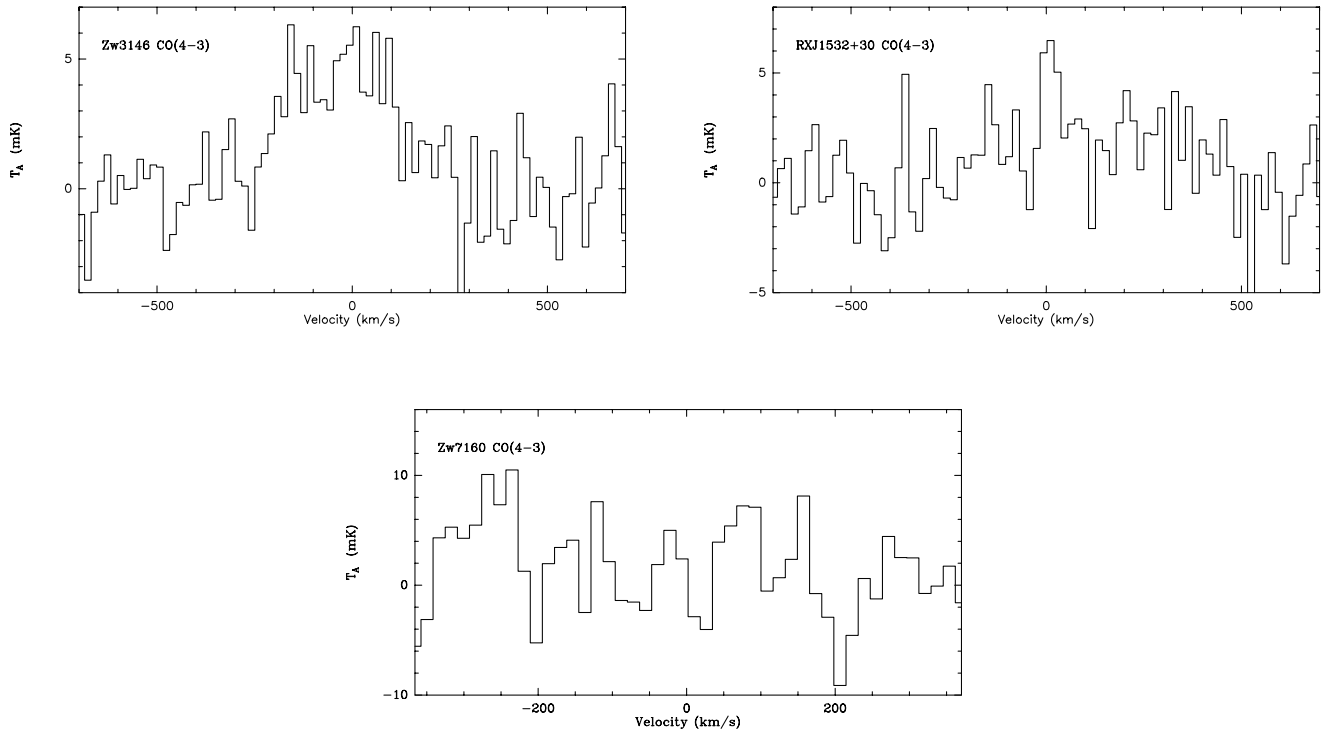

Figure 2. JCMT CO(4–3) spectra for Zw 3146, RX J1532+30 and Zw 7160. Note the much smaller bandwidth used in the archival Zw 7160 observation.

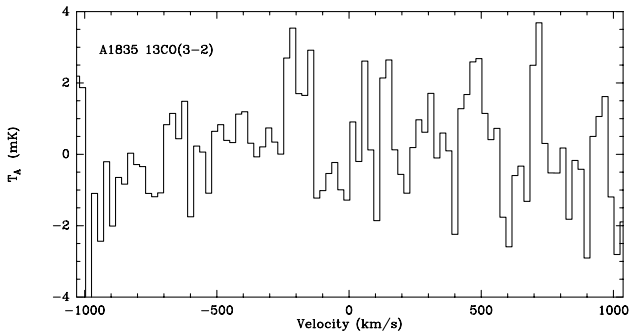

Figure 3. JCMT spectrum for A1835 ^{13}CO(3–2).

Table 7. Summary of IRAM results for non-zero continuum levels.

Cluster	Frequency (GHz)	Continuum (mK)	Continuum (mJy)
RX J0439+05	95.423	13 ± 4	70 ± 22
RX J0747–19	104.054	3 ± 1	16 ± 5
A646	102.300	3 ± 1	16 ± 5
4C+55.16	92.811	23 ± 4	124 ± 22
Hydra A	109.382	47 ± 4	254 ± 22
Zw 8193	97.210	3 ± 1	16 ± 5
Zw 8276	107.179	3 ± 1	16 ± 5
A2390	93.853	3 ± 1	16 ± 5

observation, but is strong enough to lead us to claim without confirmation. The continuum level detected implies a flat ($\alpha = -0.4$) radio source from 1 to 100 GHz.

A291. No line was found for this relatively anonymous system which is amongst the least optical line-luminous systems observed. Our upper limit lies above the line that marks the highest molecular mass detections.

A11. This cluster was included in this study owing to its remarkably strong optical emission line spectrum (Perlman et al. 1998). The IRAM data were taken in service time during relatively poor conditions, but show a line at the same frequency at two different tunings.

Overall we have seven high-significance CO(1–0) detections, which have additional CO(2–1), CO(3–2) or CO(4–3) detections, and another nine CO(1–0) detections that are close to the limit of detectability with IRAM but are confirmed with repeat observations. Even if several of our tentative detections prove to be spurious, these observations represent more than an order of magnitude increase in the number of CO detections for cooling flows. The prospects for increasing this number of detections further may be limited, as the number of systems with strong optical emission lines is relatively small and we have observed the vast majority of these in this study.

We have calculated molecular gas masses from the relationship used by Sanders, Scoville & Soifer (1991), which includes a factor of 1.36 to account for the contribution of helium to the total gas mass:

$$M(\mathrm{H_2}) = 1.18 \times 10^4 S(\mathrm{CO}) d_{\mathrm{Mpc}}^2 \, \mathrm{M_\odot},$$

where S(CO) is the integrated flux density of the line (Jy km s^{-1}) determined from the measured antenna temperature (T_{A}^*) using $6.8(1+z)^{-1/2}$ Jy K^{-1} for IRAM, and d_{Mpc} is the luminosity distance to the cluster. This conversion excludes the factor of 1.36 to account for the contribution of helium to the total gas mass. We use molecular gas mass throughout this paper. With one exception, this formula agrees with all other quoted conversion factors in previous cooling flow CO search papers (Ulmer & Grabelsky 1990; McNamara & Jaffe 1994; O'Dea et al. 1994; Braine & Dupraz 1994; Fujita et al. 2000) to within 20 per cent, taking into account

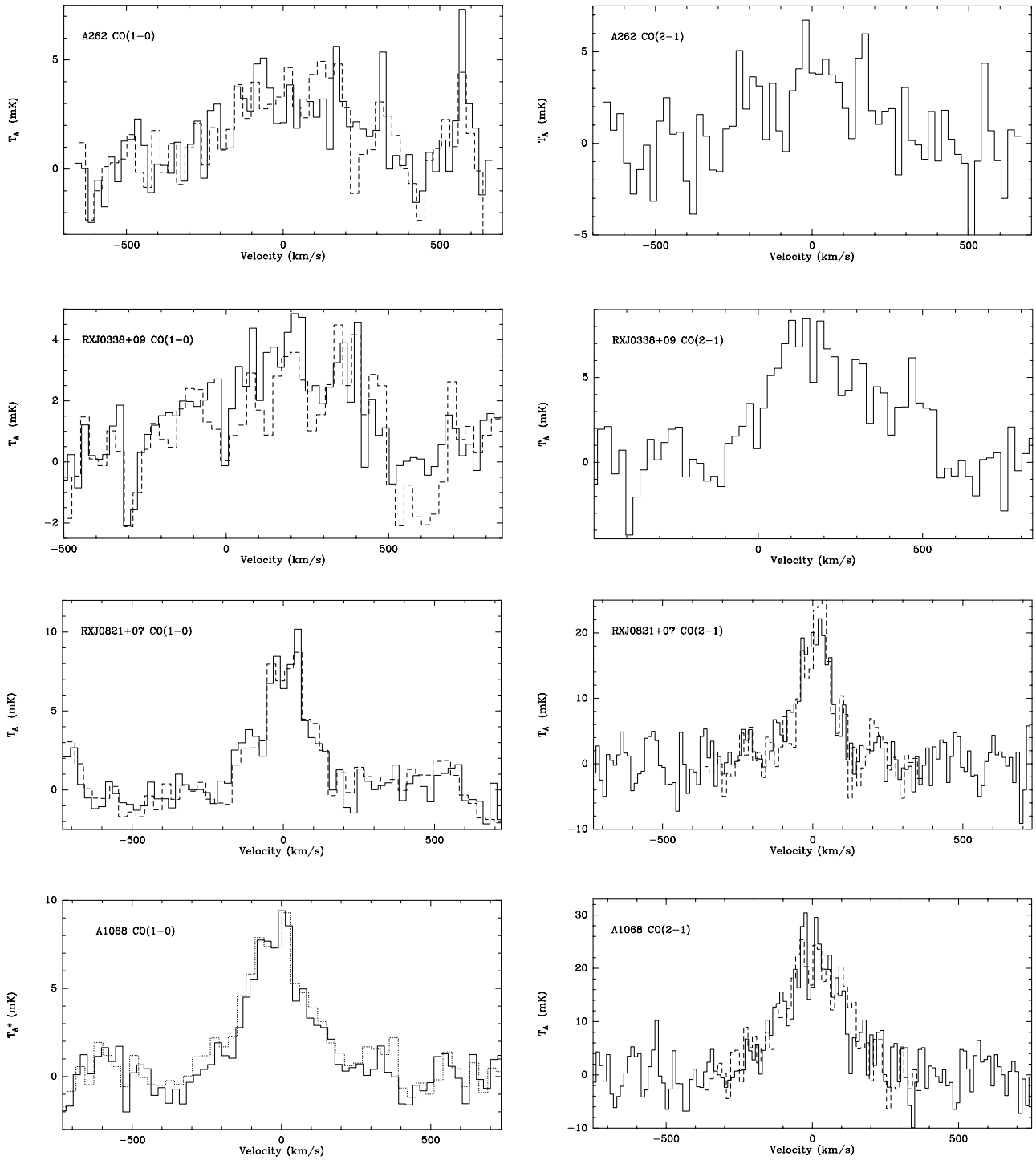

Figure 4. IRAM 30-m spectra for CO(1–0) and CO(2–1) for A262, RX J0338+09, RX J0821+07 and A1068. The solid line shows the coadded 500-MHz data from A100 and B100, and the dashed or dotted line shows the coadded autocorrelator data from A100 and B100.

differences in H_0, the use of a simple approximation about beam area that does not correctly account for $(1 + z)$ effects, the number of σ to which the results are quoted, the assumed width of the undetected line, the beamsize, the Galactic CO to H_2 conversion factor [Sanders et al. use $3 \times 10^{20}\,\mathrm{cm}^{-2}\,(\mathrm{K\,km\,s}^{-1})^{-1}$] and the use of beam efficiencies [0.842 was used for all IRAM 30-m CO(1–0) observations]. The exception is the study by O'Dea et al. (1994), where the gas mass limits are a factor of 4 too low given the formula that they quote in equation (4) compared with the comparable one in Braine & Dupraz (1994). This discrepancy arises because of the incorrect use of a radius rather than a diameter in these calculations (O'Dea, private communication). Given the cumulative uncertainties in all these previous papers, we present a direct calculation *using the same assumptions* for all previous papers (including O'Dea et al. 1994) in Table 8 for comparison with our results.

Clearly these crude conversions may not be appropriate in the cooling flow systems, so they should be viewed very much as a

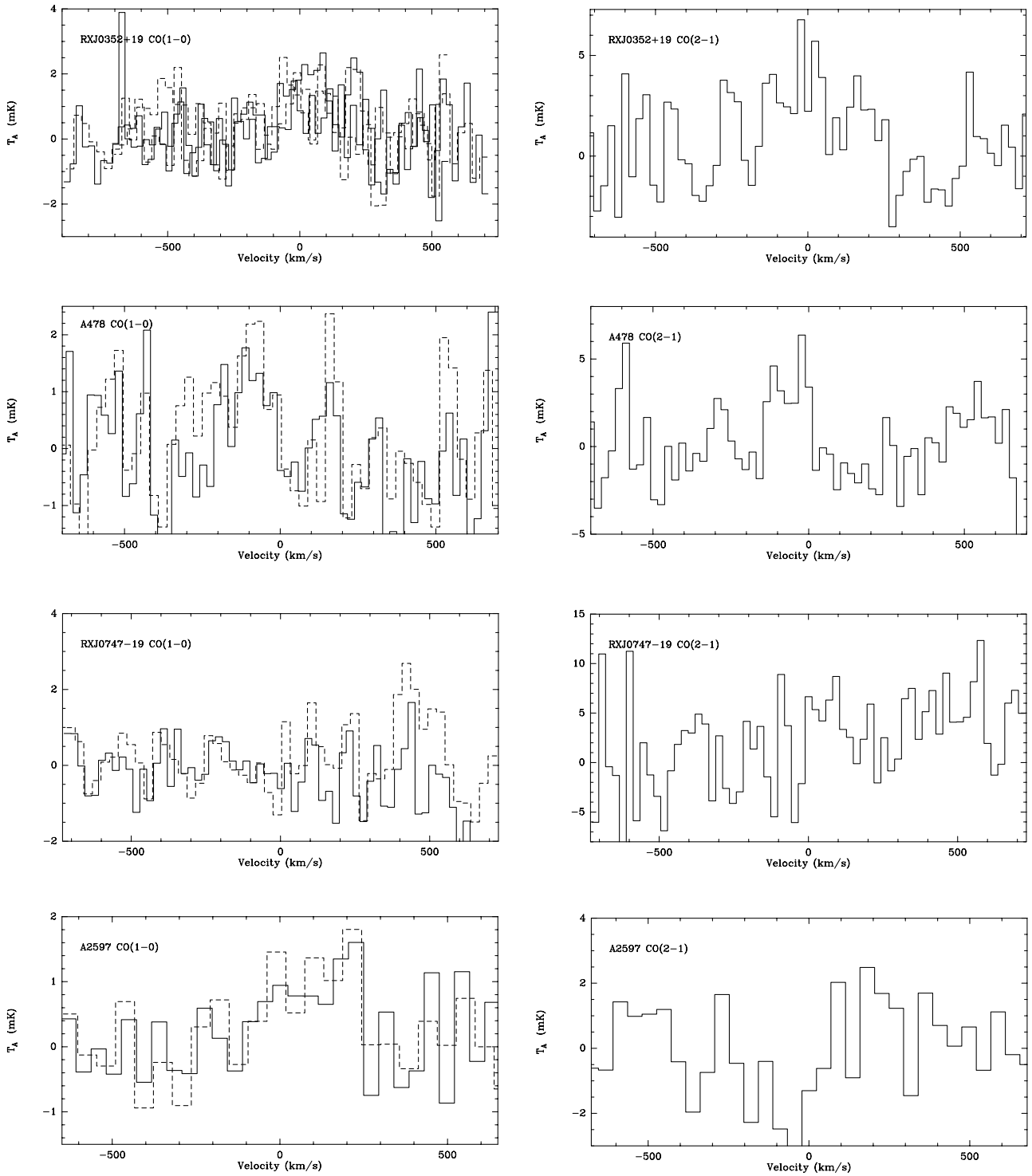

Figure 5. IRAM 30-m spectra for CO(1–0) and CO(2–1) for RX J0352+19, A478, RX J0747–19 and A2597. The solid line shows the coadded 500-MHz data from A100 and B100, and the dashed line shows the coadded autocorrelator data from A100 and B100. The plot for RX J0352+19 contains data from two frequency-shifted observations. The data for A2597 are smoothed more heavily than the other spectra to show the weak feature in both spectra.

guideline. For warmer gas than in the Galaxy we could overestimate [e.g. in ultraluminous infrared galaxies, Solomon et al. (1997) claim a factor of 4 overestimate]. If the gas is colder ($<$10 K), then this relationship could be substantially underestimated. Whichever is the case, the overall proportions will scale between the galaxies in the sample. The values that we calculate are presented in Table 9 with other relevant parameters and other data from the literature. Overall these observations give molecular gas mass estimates in the range 8×10^{8} to 2.5×10^{11} $M_{\odot}$.

5 DISCUSSION

The detection of CO in 16 massive cooling flows, and sensitive limits on a further 13, has significant implications for our

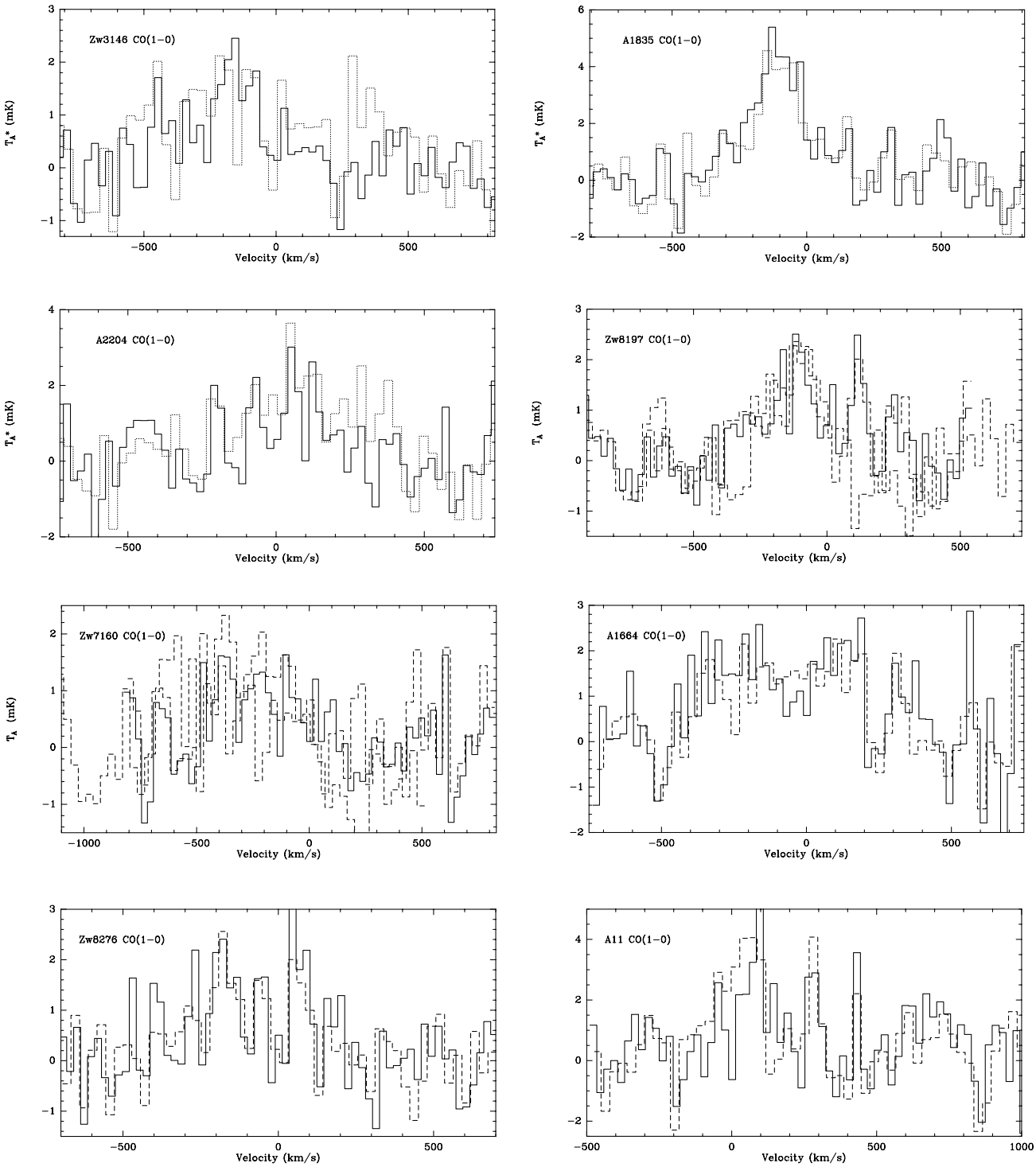

Figure 6. IRAM 30-m spectra for Zw 3146, A1835, A2204, Zw 8197, Zw 7160, A1664, Zw 8276 and A11, where only CO(1–0) was observed because of redshift or weather constraints. The lines are as described in Fig. 4.

understanding of the deposition of matter in the cores of these systems.

5.1 Previous observations

The first question posed by our results is: why have not more cooling flows been found to contain molecular gas? The principal reason for this lies in the small number of extreme cooling flows that lie within a redshift of 0.1. Perseus/NGC 1275 is the only cooling flow at $z < 0.1$ with a central galaxy having an optical line luminosity in excess of $10^{42}\,\mathrm{erg\,s^{-1}}$ to have been observed and detected at CO(1–0) (see Bridges & Irwin 1998). The only other such system to have been studied is PKS 0745–191 (O'Dea et al. 1994). If a common mechanism lies behind the excitation of optical lines and warming of molecular gas, either by the ultraviolet continuum of massive stars (Allen 1995; Crawford et al. 1999) or

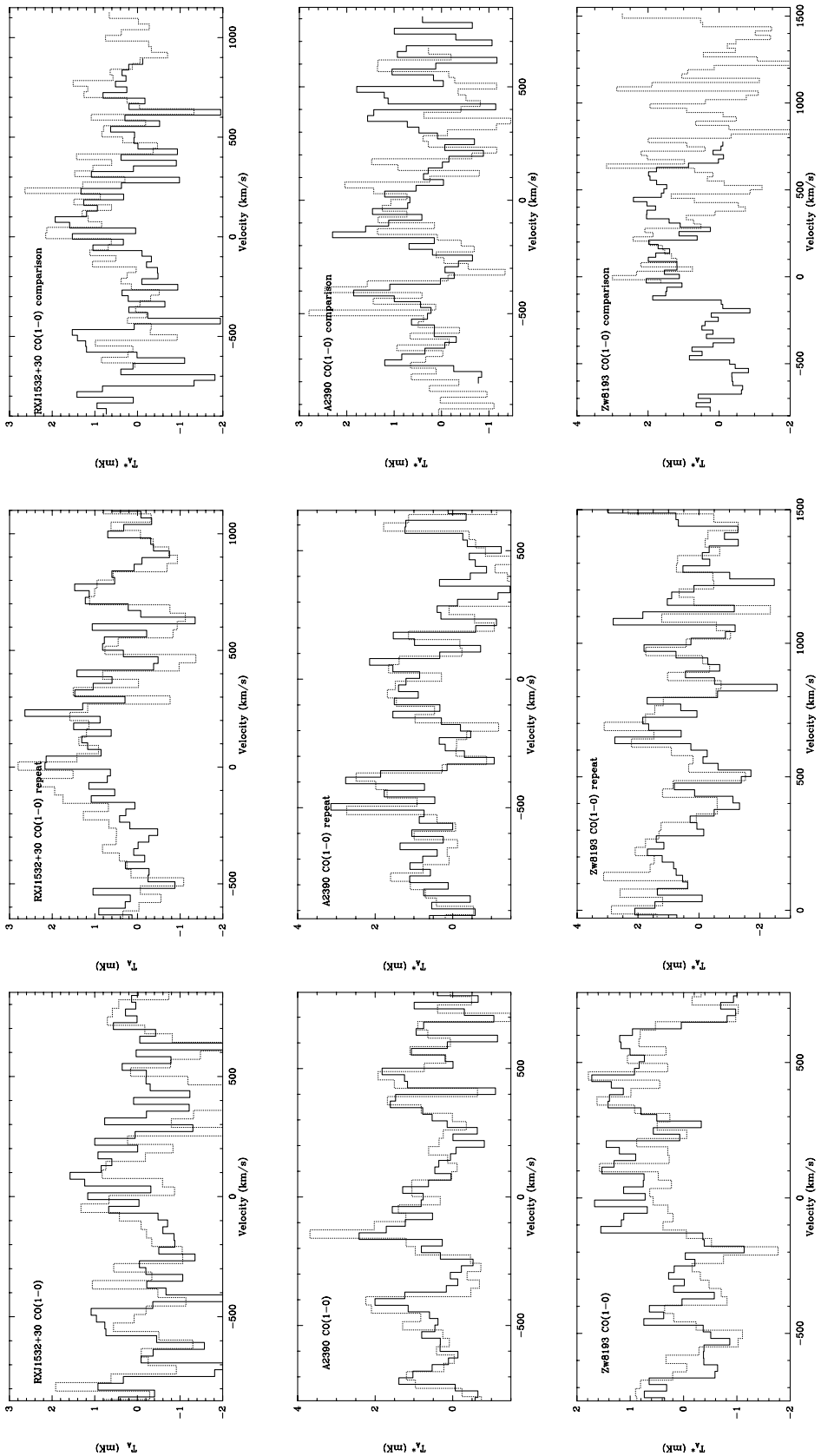

Figure 7. IRAM 30-m spectra for RX J1532+30, A2390 and Zw 8193 which were observed several times. The left and central plots of each line are as in Fig. 4. In the right-hand plots the solid line shows the 500-MHz data for the first observation and the dotted line shows the 500-MHz data for the second observation. Note the change in velocity range between observations.

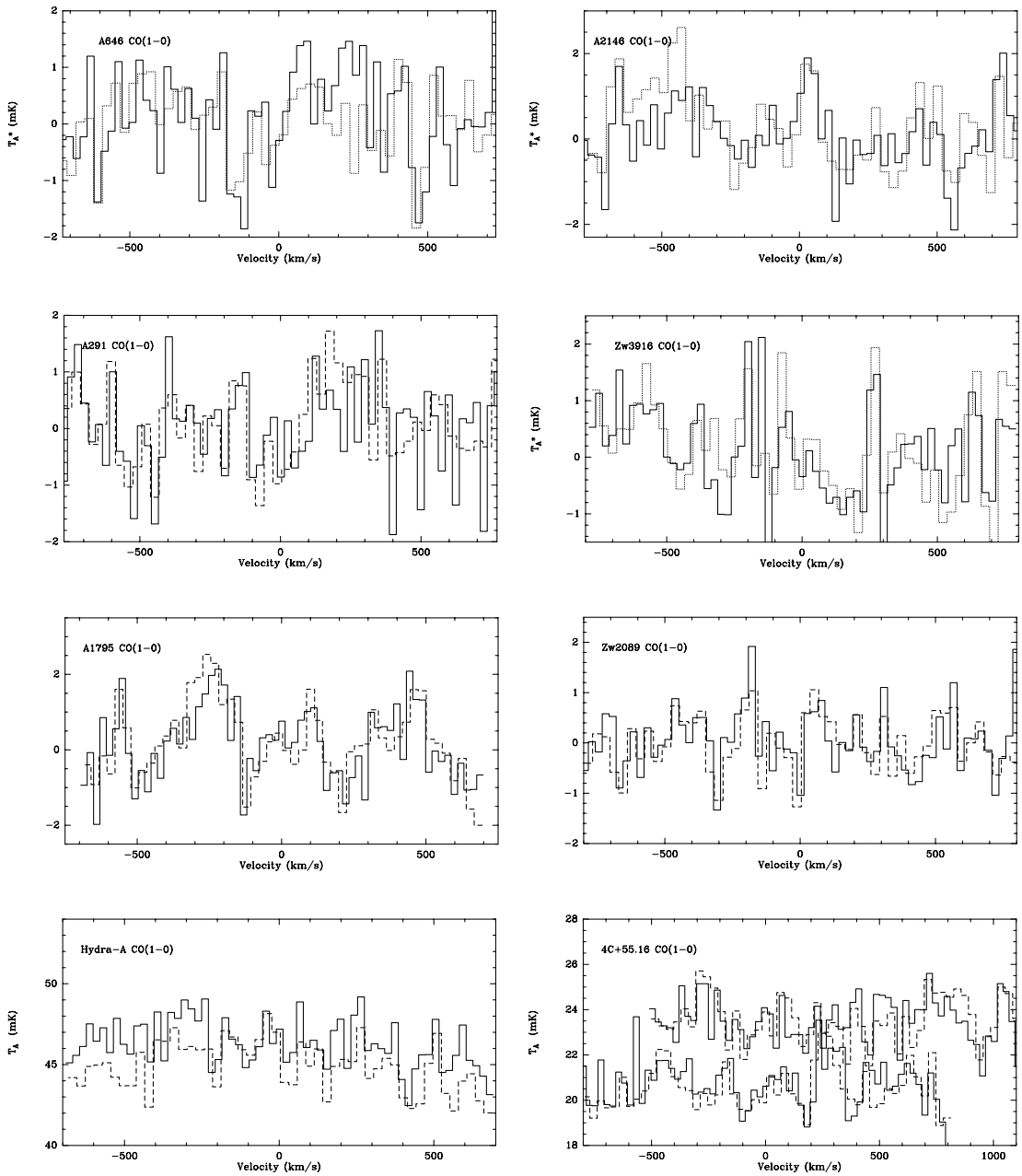

Figure 8. IRAM 30-m spectra for A646, A2146, A291, Zw 3916, A1795, Zw 2089, Hydra A and 4C+55.16 which were only observed once, and no significant detection made. Note the change in the continuum level between observations of 4C+55.16, which is probably due to small pointing differences. The lines are as described in Fig. 4.

by X-ray excitation (Voit & Donahue 1995; Wilman et al. 2001), then the luminosity of the two should be related linearly. Fig. 9 shows the mass of molecular gas plotted against Hα luminosity for our detections and upper limits, plus NGC 1275 and 3σ upper limits from Grabelsky & Ulmer (1990), McNamara & Jaffe (1992), O'Dea et al. (1994) and Braine & Dupraz (1994). We also plot the recent detections of CO in 3C 31 (the central galaxy in an X-ray-luminous group and part of the BCS sample) and 3C 264 (the dominant galaxy in A1367, also in the BCS sample) of Lim et al. (2001), which are very different in appearance (double-peaked velocity profiles) but comparable in molecular hydrogen mass. While most of the plot is unconstrained, it is clear that the most line-luminous sources are more likely to be found in current CO searches, and a linear relation between molecular gas and emission-line luminosity is consistent with the data. The relationship plotted in Fig. 9 is of one luminosity against another, so care must be taken in interpreting it. That said, this paper presents data on a complete sample of luminous optical line emission systems ($L_{\mathrm{H}\alpha} > 10^{41.5}\,\mathrm{erg\,s^{-1}}$), where 11 out of 21 are detected and only two systems have upper limits below the scatter in the detected objects (PKS 0745–191 and RX J0439+05, which both host powerful radio sources). Therefore the observed correlation holds for the majority of luminous optical line systems and is not an artefact. If this relation holds then previous surveys may have only *just* missed detecting CO. The effect of the beamsize compared with the possible size of the CO emission ($<$40 kpc for $z < 0.1$ for most observations) and the use of a smaller telescope diameter also act to weaken the limits set by

Table 8. Summary of derived parameters from previous papers. All intensities are corrected for beam efficiency and assume a linewidth of 300 km s^{-1}. The limits derived from CO(2–1) data assume CO(2–1)/CO(1–0) of 0.6 as used by McNamara & Jaffe (1994). The mass flow rates are taken from Peres et al. (1998) or White, Jones & Forman (1997). The optical line luminosities are from Crawford et al. (1999), the compilation of Heckman et al. (1989) or Owen, Ledlow & Keel (1995). References: Jaffe (1987) – J87; Bregman & Hogg (1988) – BH88; Ulmer & Grabelsky (1990) – UG90; McNamara & Jaffe (1994) – MJ94; Braine & Dupraz (1994) – BD94; O'Dea et al. (1994) – O94; Fujita et al. (2000) – F00; Lim et al. (2001) – L01.

Cluster	Reference	Telescope	Line	Beam diameter (arcsec)	3σ intensity limit (K km s^{-1})	Molecular gas mass	Mass flow rate ($M_\odot$ yr^{-1})	Optical line luminosity (erg s^{-1})
M87	J87	NRAO-12m	CO(1–0)	56	<1.35	$<1.3\times10^{8}$	–	1.1×10^{40}
MKW1	BH88	NRAO-12m	CO(1–0)	56	<0.35	$<1.6\times10^{9}$	–	–
R0338+096	BH88	NRAO-12m	CO(1–0)	56	<0.45	$<5.5\times10^{9}$	325	1.0×10^{41}
A1126	BH88	NRAO-12m	CO(1–0)	59	<0.12	$<3.6\times10^{9}$	–	5.4×10^{41}
A2199	BH88	NRAO-12m	CO(1–0)	56	<0.30	$<2.9\times10^{9}$	154	3.5×10^{40}
A262	UG90	NRAO-12m	CO(1–0)	56	<1.24	$<3.3\times10^{9}$	27	6.0×10^{39}
A496	UG90	NRAO-12m	CO(1–0)	56	<0.81	$<9.3\times10^{9}$	95	3.4×10^{40}
A978	UG90	NRAO-12m	CO(1–0)	59	<1.27	$<4.8\times10^{10}$	–	$<2\times10^{40}$
A1126	UG90	NRAO-12m	CO(1–0)	59	<0.65	$<3.8\times10^{10}$	–	5.4×10^{41}
A1185	UG90	NRAO-12m	CO(1–0)	57	<0.83	$<1.1\times10^{10}$	0	$<5\times10^{39}$
A1795	UG90	NRAO-12m	CO(1–0)	58	<0.57	$<2.4\times10^{10}$	381	1.1×10^{41}
A1983	UG90	NRAO-12m	CO(1–0)	57	<1.00	$<2.2\times10^{10}$	6	$<7\times10^{39}$
A2052	UG90	NRAO-12m	CO(1–0)	57	<1.78	$<2.3\times10^{10}$	125	4.8×10^{40}
A2199	UG90	NRAO-12m	CO(1–0)	56	<1.49	$<1.4\times10^{10}$	154	3.5×10^{40}
A2319	UG90	NRAO-12m	CO(1–0)	58	<0.56	$<1.7\times10^{10}$	20	$<1\times10^{41}$
R0338+096	UG90	NRAO-12m	CO(1–0)	56	<0.59	$<7.1\times10^{9}$	325	1.0×10^{41}
Hydra A	MJ94	JCMT-15m	CO(2–1)	22	<0.55	$<4.5\times10^{9}$	264	1.6×10^{41}
A1060	MJ94	JCMT-15m	CO(2–1)	21	<0.96	$<4.1\times10^{8}$	15	
MKW3s	MJ94	JCMT-15m	CO(2–1)	22	<0.42	$<2.3\times10^{9}$	175	$<5\times10^{39}$
A2151	MJ94	JCMT-15m	CO(2–1)	22	<0.61	$<2.1\times10^{9}$	166	$<5\times10^{39}$
A2256	MJ94	JCMT-15m	CO(2–1)	22	<0.94	$<9.5\times10^{9}$	0	$<5\times10^{40}$
Cygnus A	MJ94	JCMT-15m	CO(2–1)	22	<0.99	$<9.0\times10^{9}$	244	6.5×10^{42}
A262	BD94	IRAM-30m	CO(1–0)	21	<0.60	$<3.1\times10^{8}$	27	6.0×10^{39}
A262	BD94	IRAM-30m	CO(2–1)	11	<1.05	$<2.3\times10^{8}$	27	6.0×10^{39}
R0338+096	BD94	IRAM-30m	CO(1–0)	22	<0.66	$<1.5\times10^{9}$	325	1.0×10^{41}
R0338+096	BD94	IRAM-30m	CO(2–1)	11	<0.93	$<9.3\times10^{8}$	325	1.0×10^{41}
A478	BD94	IRAM-30m	CO(1–0)	23	<0.45	$<7.3\times10^{9}$	616	1.1×10^{41}
A478	BD94	IRAM-30m	CO(2–1)	11	<0.90	$<6.1\times10^{9}$	616	1.1×10^{41}
Hydra A	BD94	IRAM-30m	CO(1–0)	22	<0.66	$<3.9\times10^{9}$	264	1.6×10^{41}
Hydra A	BD94	IRAM-30m	CO(2–1)	11	<0.87	$<2.1\times10^{9}$	264	1.6×10^{41}
A1795	BD94	IRAM-30m	CO(1–0)	22	<0.54	$<4.4\times10^{9}$	381	1.1×10^{41}
A1795	BD94	IRAM-30m	CO(2–1)	11	<0.87	$<3.0\times10^{9}$	381	1.1×10^{41}
A2029	BD94	IRAM-30m	CO(1–0)	23	<0.45	$<5.7\times10^{9}$	556	$<8\times10^{39}$
A2029	BD94	IRAM-30m	CO(2–1)	11	<1.11	$<5.8\times10^{9}$	556	$<8\times10^{39}$
A2052	BD94	IRAM-30m	CO(1–0)	22	<0.39	$<9.7\times10^{8}$	125	4.8×10^{40}
A2052	BD94	IRAM-30m	CO(2–1)	11	<0.24	$<2.5\times10^{8}$	125	4.8×10^{40}
A2199	BD94	IRAM-30m	CO(1–0)	22	<0.54	$<1.0\times10^{9}$	154	3.5×10^{40}
A2199	BD94	IRAM-30m	CO(2–1)	11	<0.69	$<5.3\times10^{8}$	154	3.5×10^{40}
P0745–19	O94	SEST-15m	CO(1–0)	47	<0.57	$<4.2\times10^{10}$	1038	2.9×10^{42}
Hydra A	O94	SEST-15m	CO(1–0)	45	<0.66	$<1.3\times10^{10}$	264	1.6×10^{41}
A3526	O94	SEST-15m	CO(1–0)	43	<0.66	$<5.0\times10^{8}$	30	5.0×10^{39}
A3526	O94	SEST-15m	CO(2–1)	22	<1.80	$<5.6\times10^{8}$	30	5.0×10^{39}
AWM7	F00	NRO-45m	CO(1–0)	15	<1.39	$<3.5\times10^{8}$	41	$<5.0\times10^{39}$
RX J0107+32	L01	IRAM-30m	CO(1–0)	22	3.74 ± 0.49	$2.2\pm0.3\times10^{9}$	–	5.0×10^{39}
A1367	L01	IRAM-30m	CO(1–0)	22	0.55 ± 0.10	$5.2\pm1.0\times10^{8}$	–	4.0×10^{39}

previous observations. The high detection rate for CO in this paper is largely due to the selection of the newly discovered line-luminous systems found in the *ROSAT* All Sky Survey (Crawford et al. 1999) which draws massive cooling flows from a much larger volume, and the smaller beamsize provided by the IRAM 30-m.

An additional factor that can account for some of the observed differences is the fact that the velocity shifts seen in our data were not accounted for in previous studies, so some detections may have been overlooked in the past. Indeed, inspection of the spectra of Braine & Dupraz (1994) shows possible detections of A262, A478 and 3A0335+09 with $\approx$200 km s^{-1} offset from zero velocity. All three of these galaxies are detected in our IRAM 30-m data. Although A478 is only a marginal detection, both A262 and 3A0335+09 are detected at 5–7 times the level quoted as a limit by

Table 9. Summary of derived parameters. All upper limits are 3σ. Mass flow rates are from Allen et al. (1996) and Allen (2000) and are corrected for excess absorption. The gas mass for RX J1347−11 is derived from our CO(3–2) limit assuming CO(3–2)/CO(1–0) of 0.4. The optical line luminosities are from Crawford et al. (1999) apart from A11 (Perlman, private communication), and estimates for 4C +55.19, Zw 2089, I0910+41, 3C 48 and A1367/3C 264 from inspection of published spectra. The dust masses are calculated for a dust temperature of 40 K. Note that gas-to-dust ratios are for molecular gas only and an additional factor of 1.36 is required for total gas-to-dust ratios.

Cluster	Redshift	Optical line luminosity ($\mathrm{erg\,s^{-1}}$)	Mass flow rate ($\mathrm{M_\odot\,yr^{-1}}$)	SCUBA flux at 850 μm (mJy)	*IRAS* flux at 60 μm (mJy)	Dust mass ($\mathrm{M_\odot}$)	Molecular gas mass estimate ($\mathrm{M_\odot}$)	Gas-to-dust ratio
A11	0.1503	1.0×10^{42}	–	–	100 ± 40	1.4×10^{7}	$2.6\pm0.7\times10^{10}$	1820
A262	0.0171	6.0×10^{39}	27	–	290 ± 24	4.4×10^{5}	$9.0\pm1.3\times10^{8}$	2040
A291	0.196	4.6×10^{41}	–	–	110 ± 35	2.9×10^{7}	$<2.3\times10^{10}$	<795
RX J0338+09	0.0338	1.0×10^{41}	325	–	120 ± 33	7.3×10^{5}	$3.9\pm0.4\times10^{9}$	5350
RX J0352+19	0.109	5.8×10^{41}	–	–	<99	$<6.9\times10^{6}$	$1.2\pm0.3\times10^{10}$	>1700
A478	0.0882	1.1×10^{41}	616	–	230 ± 56	1.0×10^{7}	$4.5\pm2.6\times10^{9}$	450
RX J0439+05	0.208	1.1×10^{42}	–	–	<102	$<3.1\times10^{7}$	$<3.3\times10^{10}$	–
RX J0747−19	0.1028	1.4×10^{42}	1038	–	<288	$<1.8\times10^{7}$	$<7.6\times10^{9}$	–
A646	0.1268	1.6×10^{41}	–	–	<132	$<1.3\times10^{7}$	$<1.3\times10^{10}$	–
RX J0821+07	0.110	3.0×10^{41}	–	–	300 ± 30	2.2×10^{7}	$3.9\pm0.4\times10^{10}$	1750
4C + 55.19	0.242	$\approx10^{42}$	–	–	<105	$<4.6\times10^{7}$	$<4.5\times10^{10}$	–
Zw 2089	0.235	$\approx10^{42}$	–	–	<105	$<4.2\times10^{7}$	$<4.6\times10^{10}$	–
Hydra A	0.052	1.6×10^{41}	264	–	90 ± 33	1.3×10^{6}	$<2.0\times10^{9}$	<1540
Zw 3146	0.2906	7.0×10^{42}	1358	6.6	80 ± 30	2.2×10^{8}	$1.6\pm0.3\times10^{11}$	740
A1068	0.1386	1.7×10^{42}	937	–	650 ± 39	7.7×10^{7}	$8.5\pm0.6\times10^{10}$	1110
Zw 3916	0.204	3.0×10^{41}	–	–	<123	$<3.5\times10^{8}$	$<1.6\times10^{10}$	–
A1664	0.1276	1.1×10^{42}	260	–	<159	$<1.6\times10^{7}$	$4.4\pm0.7\times10^{10}$	>2720
RX J1347−11	0.4503	3.0×10^{42}	1790	3.5	<132	1.8×10^{8}	$<6.8\times10^{10}$	<375
A1795	0.0620	1.1×10^{41}	381	–	<147	$<3.1\times10^{6}$	$<2.7\times10^{9}$	–
A1835	0.2523	1.4×10^{42}	2111	4.4	330 ± 69	1.0×10^{8}	$1.8\pm0.2\times10^{11}$	1760
Zw 7160	0.2578	5.0×10^{41}	1227	5.3	<87	1.5×10^{8}	$6.1\pm2.4\times10^{10}$	410
RX J1532+30	0.3615	4.2×10^{42}	–	–	<99	$<1.2\times10^{8}$	$2.5\pm0.4\times10^{11}$	>2110
A2146	0.2343	1.4×10^{42}	–	–	140 ± 26	5.6×10^{7}	$<3.5\times10^{10}$	<620
A2204	0.1514	1.6×10^{42}	1660	–	<297	$<4.3\times10^{7}$	$2.3\pm0.6\times10^{10}$	>540
Zw 8193	0.1825	1.5×10^{42}	–	–	<99	$<2.2\times10^{7}$	$<4.3\times10^{10}$	–
Zw 8197	0.1140	1.6×10^{41}	–	–	<87	$<6.7\times10^{6}$	$1.1\pm0.3\times10^{10}$	>1640
Zw 8276	0.0757	1.3×10^{41}	–	–	80 ± 22	2.6×10^{6}	$8.2\pm1.2\times10^{9}$	3140
A2390	0.2328	6.2×10^{41}	600	4.8	<162	9.0×10^{7}	$<4.9\times10^{10}$	<540
A2597	0.0852	5.2×10^{41}	271	–	<100	$<4.1\times10^{6}$	$8.1\pm3.3\times10^{9}$	>1990
NGC 1275	0.0184	4.7×10^{42}	556	–	35000	5.3×10^{7}	$1.7\pm0.2\times10^{10}$	323
I09104+41	0.4420	$>1\times10^{42}$	1060	<6.4	400	1.6×10^{8}	$<5.1\times10^{10}$	<319
3C 48	0.3695	$>1\times10^{42}$	300	–	761	2.0×10^{8}	$1.6\pm0.6\times10^{10}$	80
R0107+32	0.0175	6.0×10^{39}	–	–	360 ± 63	5.8×10^{5}	$2.2\pm0.3\times10^{9}$	3793
A1367	0.0218	5.0×10^{39}	0	–	160 ± 58	4.1×10^{5}	$5.2\pm1.0\times10^{8}$	1268

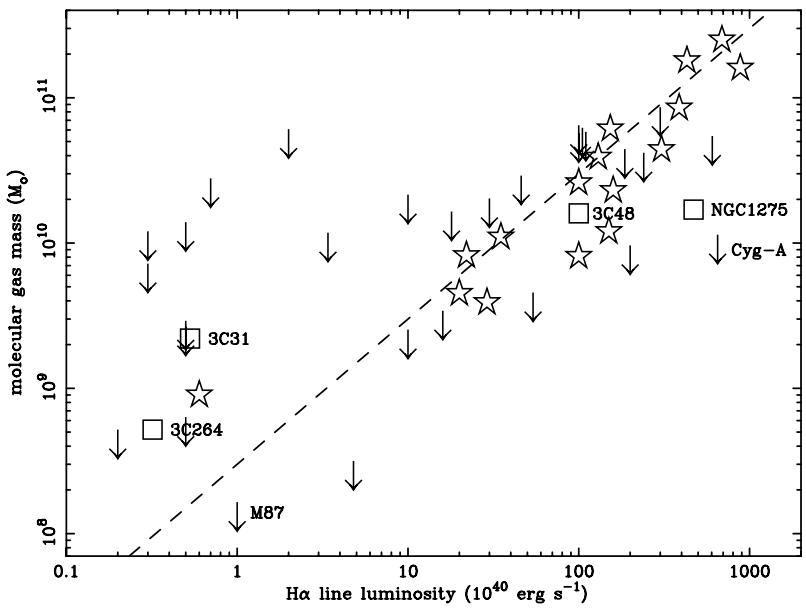

Figure 9. Molecular gas estimate plotted against optical line luminosity. The open stars are new detections presented here, the squares are detections of other central cluster galaxies, and the upper limits are from this work and the literature. The dashed line marks a line with a constant ratio of molecular gas mass to optical line emission, and is not a fit to the data.

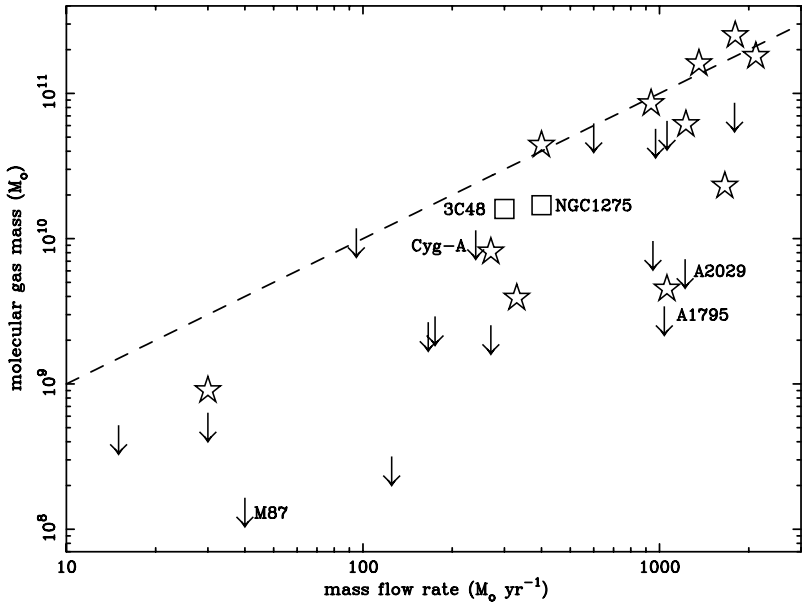

Figure 10. Molecular gas estimate plotted against global mass flow rate. The symbols and line are as in Fig. 9. Not all points are plotted, as mass flow rates are not known for all detections and upper limits.

Braine & Dupraz (1994). We can only account for this discrepancy if the authors subtracted any velocity offset emission in the baseline subtraction.

As global mass deposition rates are known for the majority of the sample presented here and all the published upper limits, we can plot the molecular gas mass against mass deposition rate (Fig. 10). This plot illustrates that there are a number of very massive cooling flows without strong optical emission lines (e.g. A478, A1795 and A2029) where the upper limits/detections on the molecular gas mass are restrictive. Fig. 10 implies that the observed mass of molecular gas is *not directly* related to the total mass deposited. There may be a correlation with the mass deposited on smaller scales ($<$50 kpc), but the high-resolution X-ray data have not yet been obtained to test this. However, the upper bound on the molecular gas mass is correlated with the mass deposition rate. This is expected if the observed molecular gas is a small percentage of the total deposited gas that is warmed by young stars or an active nucleus.

The relationship plotted in Fig. 9, although a luminosity–luminosity plot, has some predictive power if the optical line luminosity and Balmer decrement are known. For instance, all sources with an optical line luminosity less than $10^{41}\,\mathrm{erg\,s^{-1}}$ in Crawford et al. (1999) are likely to have a CO(1–0) line intensity below $0.3\,\mathrm{K\,km\,s^{-1}}$, so beyond the observable limits of the IRAM 30-m. More distant radio galaxies and other starbursts with CO detections should have a similar ratio of CO to Hα as observed here.

There is one other factor that also plays a role: the overall radio power. There are a number of central cluster galaxies with luminous optical line emission that should be detectable using the relationship in Fig. 9 (e.g. PKS 0745−191, Hydra A, Cygnus A) but are so far undetected. Of the eight most radio powerful radio sources ($>2\times10^{25}\,\mathrm{W\,Hz^{-1}}$ at 1.4 GHz), only 3C 48 is detected, even though several of them have CO limits an order of magnitude below the level of detections at the same Hα luminosity. This could be caused by an additional optical line contribution powered by the radio source, as is clearly the case in 3C 48 which has broad Hα (Jackson & Browne 1991). In the less extreme cases the radio source and optical line morphologies do correspond (e.g. PKS 0745–191, Donahue et al. 2000), so the line emission in these systems may be directly powered (at least in part) by the radio source and hence the relationship in Fig. 9 does not hold. Alternatively, these powerful radio systems could have greater linewidths ($>$600 km s^{-1}), making detection in a 1000 km s^{-1} bandwidth virtually impossible. A broad line with a substantial integrated intensity would barely peak above the noise, so the quoted limits are for a narrow line *only* and a much larger molecular gas mass could be present. Importantly, these powerful radio galaxies are still detected in ro-vibrational H_2 lines in the infrared (Jaffe & Bremer 1997; Falcke et al. 1998; Wilman et al. 2000), so molecular gas is present despite the non-detection in CO. One final explanation is that the radio source evaporates the cold clouds, as proposed by Soker et al. (2001). While this view is difficult to reconcile with the detection of infrared H_2 lines, it cannot be dismissed with the current data. Future large-bandwidth CO observations will help to differentiate between these possibilities. The lack of CO in powerful radio systems accounts for many of the previous non-detections.

5.2 Are we detecting the cold 'sink'?

The relationship between the observed warm molecular gas and the 'sink' of cold material that should form out of the cooling flow is not immediately obvious from our observations and the wealth of previous limits on 'cold' material in cluster cores. Given recent *XMM-Newton* X-ray observations that appear to show a deficit of X-ray line emission from the coolest gas components in several strong cooling flows (Tamura et al. 2001; Peterson et al. 2001), and recent *Chandra* observations indicating that cooling flows do not extend to large radii and have characteristic time-scales of $\sim10^9$ yr (Allen et al. 2001), there is a renewed debate on this issue (see Fabian et al. 2001a).

Taking previous X-ray observations at face value and assuming that the observed molecular gas is the only molecular component in

the cooling flow, then it is not possible to account for more than 5–10 per cent of the deposited material in any of our 16 CO-detected cooling flows. This apparent contradiction can be explained if the observed molecular gas is only visible because of the warming influence of either star formation in the central galaxy or the strongly peaked X-ray emission. In these two cases, most of the material would remain unobservable in clouds of very low temperature (<10 K) in systems without star formation or a strong X-ray peak and/or at larger radii. The theoretical support for this view is divided (Ferland et al. 1994; Voit & Donahue 1995), and the most direct evidence for the cold sink is the observed intrinsic X-ray absorption seen in clusters (White et al. 1991; Allen 2000). This absorption is consistent with the presence of a column density of $10^{20.5–22}$ cm^{-2}. These levels are within an order of magnitude of the derived column densities of H_2 from our CO detections, and our stronger CO detections are in systems that are known to have intrinsic X-ray absorption (Allen 2000). Allen et al. (2001) and Allen (2000) discuss the fate of the luminosity absorbed and re-processed by this intrinsic X-ray-absorbing column.

On the other hand, the new X-ray observations point to lower mass deposition rates by factors of 2 to 5 and shorter time-scales by factors of 2 to 4, so the estimates of deposited mass could come down by factor as much as 20. This would then give, for the first time, a match in the predicted and observed cold gas masses even with the substantial uncertainties introduced by using a standard CO-to-H_2 conversion. Without obtaining the spatial extent of the CO emission, it is not yet possible to prove that the cold gas found here is as concentrated as X-ray observations predict (<50 kpc). Future X-ray observations and millimetre interferometry will address this question directly. There is a possibility that the molecular gas detected in this study is the sum total of the mass deposited in a cooling flow, but a great deal of work remains to be done before this can be proven beyond reasonable doubt.

5.3 NGC 1275 – the prototype?

The detection of molecular gas in systems other than NGC 1275 throws into question the argument that the presence of molecular gas is unrelated to the cooling flow (see Bridges & Irwin 1998 for a discussion). If the molecular gas found in cooling flows is deposited through mergers with gas-rich members, how can 10^{11} M$_\odot$ of gas be present in the most massive flows observed? When only one system is known, particularly one as outwardly peculiar as NGC 1275, then a merger is consistent with the available facts. However, when a set of galaxies with the same X-ray characteristics share the same properties (strong optical emission lines and CO emission), then some common causal relationship other than infrequent mergers must be invoked. The connection between low central cooling times measured from X-ray imaging and the presence of optical lines (Peres et al. 1998) points to a causal link between cooling gas and the presence of irradiated cold clouds. Any model invoking mergers in all cases has to explain the high fraction of massive cooling flows with CO emission in clusters with relatively few spiral galaxy members.

Our results should also prompt us to reconsider the properties of NGC 1275. The presence of dust, strong optical emission lines and a powerful radio source are features found in many central cluster galaxies in the most massive cooling flows. The presence of young star clusters like the ones found in NGC 1275 (Holtzman et al. 1992; Zepf et al. 1995) is hinted at in the strong Balmer series seen in the integrated spectra of some galaxies (Crawford et al. 1999). As yet, imaging data have not resolved these young stars into clusters, but further *HST* imaging could do so.

5.4 Linewidths

The velocity width of the detected CO lines is another important factor. Our detections are all of systems with widths less than 500 km s^{-1}, implying that the gas is localized to galaxy-scale regions and is not virialized in the cluster core. Taking all 16 of our detections, the systemic velocity shifts relative to the published optical line redshift have a mean of -7 km s^{-1} and an rms of 130 km s^{-1}. Given the errors in the optical velocities, these values are consistent with the warm molecular gas coming from a small number of regions of intense star formation drawn from the underlying velocity dispersion of the central galaxy. The velocity discrepancies and small linewidths are similar to those seen in other radio galaxies with CO detections (e.g. 3C 293: Evans et al. 1999).

The underlying dispersion could be underestimated if the restricted bandwidth available results in individual clouds on a high-velocity 'tail' of this distribution being missed entirely, thus lowering the rms calculated above. Future large-bandwidth observations would detect any such high-velocity clouds.

The linewidths can also be used to determine crude dynamical mass estimates on the somewhat sweeping assumption that the molecular gas is in a disc (Carilli, Menten & Yun 1999; Papadopoulos et al. 2000). Without direct measurement of the extent of the CO emission, the disc diameter is a free parameter. For $M_{\rm dyn} \approx M_{\rm H_2}$, the disc diameters would range from 1 to 5 kpc. If future interferometry of these systems finds larger sizes, then this would be another example of the 'excess mass' problem (Carilli et al. 1999) where the gas mass exceeds the dynamical mass in nuclear starbursts.

At the opposite extreme, lines with large velocity widths (>800 km s^{-1}) would be difficult to detect even with our 1.8-GHz bandwidth JCMT data, owing to the baseline subtraction method used. Changing the velocity ranges for the baseline subtraction makes no significant difference to the results for the narrow lines, but some emission could be missed if a broad line were present. Such broad lines, although weak in peak intensity, could easily reach 2–5 K km s^{-1} and account for in excess of 5×10^{11} M$_\odot$ of gas if warm. Any broad lines are likely to be from colder gas clouds further from any star formation or intense X-ray emission, so the CO(1–0) emission will be considerably weaker than that from the >30 K gas. Work by Antonucci & Barvainis (1994) demonstrates that large-bandwidth observations can be made by splicing together smaller bandwidths, but none of the five clusters that they observed contained a strong optical line emission system so it is difficult to compare their results with ours. Future large-bandwidth receivers will provide the data required to detect such broad features, although the low temperature of the gas may limit the chances of detection. Current technology is well suited to detecting narrower CO lines which are reasonably warm.

5.5 Time-scales

If one assumes that the systems we are observing are in a steady state then the observed molecular gas mass should reflect the balance of mass deposition and star formation rates. Following the argument of Braine & Dupraz (1994), one can determine the likely time-scale for gas to be held in clouds before forming stars. While most of the clusters in this sample do not have accurate and

high-resolution X-ray imaging, and the true extent of the molecular gas is unknown, it is difficult to derive the true ratio of total mass to mass deposition rate. However, in the case of A1068 and A1835 we can derive values of the mass deposition rate of 150 and $500\,M_\odot\,yr^{-1}$ at 50 kpc from the deprojection results of Allen (2000). In both of these systems, Crawford et al. (1999) quote apparent star formation rates (31 and $125\,M_\odot\,yr^{-1}$) which imply that the efficiency of forming stars (η_{SF}) is of the order of 0.2. This efficiency is close to that used by Braine & Dupraz (1994). Given the total molecular mass present of 8×10^{10} and $1.8\times10^{11}\,M_\odot$, the implied time-scales for gas consumption are therefore 5×10^8 and 4×10^8 yr respectively. So, in these very central regions, the directly observed star formation rates imply that *with no further deposition* the detected molecular gas would be used up on a time-scale of less than 10^9 yr, but in every case the observed deposition exceeds the star formation rate so the time-scales could be comparable to the Hubble time. Therefore the extreme star formation seen in this sub-sample of central cluster galaxies could be a long-lived phenomenon in which a substantial fraction of the stellar population is produced. Only when CO mapping and high-resolution X-ray imaging are available for more of this sample will the issue of time-scales be clarified.

5.6 Dust

When viewed with the recent detection of dust emission in the submillimetre for A1835 and A2390 (Edge et al. 1999), the masses of molecular gas implied here for them are slightly higher than galactic gas-to-dust ratios (900 ± 200 and 350 ± 150) would suggest. Recent SCUBA detections of Zw 3146 and Zw 7160 imply a dust mass of $2.2\times10^8\,M_\odot$ and a detection of $1.5\times10^8\,M_\odot$ respectively (Chapman et al. 2001), giving gas-to-dust ratios of 740 ± 150 and 410 ± 160. The claimed Sunyaev-Zel'dovich (S–Z) effect detection at 850 μm with SCUBA of RX J1347−11 (Komatsu et al. 1999) is complicated by the detection of a central source of 3.5 mJy or $1.8\times10^8\,M_\odot$ of dust. This implies a gas-to-dust ratio of <500 from our JCMT CO(3–2) limit [assuming CO(3–2)/CO(1–0) = 0.4 and no radio source or S–Z contribution]. Finally, IRAS 09104+4109 was recently observed with SCUBA by Deane & Trentham (2001), who claim that this source lacks cold dust. Their 3σ upper limit of 6.4 mJy at 850 μm is consistent with $<3.2\times10^8\,M_\odot$. This limit would not be sufficient to detect any other known cooling flow with dust so, until substantially deeper SCUBA photometry is obtained, it cannot be claimed that IRAS 09104+4109 is deficient in cold dust.

The gas-to-dust ratios derived for this sample show a similar dispersion to that seen in other classes of galaxies. Assuming a dust temperature of 40 K, we can also estimate dust masses from the few *IRAS* detections and upper limits derived from the XSCANPI package at the Infrared Processing and Analysis Center (IPAC; Table 9). The derived gas-to-dust ratios are strongly dependent on the dust temperature used, but agree with those from submillimetre detections and limits. For the joint CO and SCUBA/*IRAS* detections including NGC 1275 but excluding 3C 48, the average gas-to-dust ratio is 1720 with a dispersion of 1410. The few very high gas-to-dust ratios (e.g. RX J0338+09 at 5350) are probably an indication that the assumption of a dust temperature of 40 K is incorrect, and to obtain ratios of 500–1000 requires dust temperatures of around 30 K. Given the number of CO detections presented here, it will be important to obtain SCUBA limits on dust masses for them. The dust temperature derived by Edge et al. (1999) of 30–50 K is comparable to the observed excitation temperatures of CO and those expected in other extragalactic systems undergoing star formation. The two possible exceptions to this are IRAS 09104+4109 (see Deane & Trentham 2001) and 3C 48 where the dust temperature is probably substantially higher than 40 K, so most of the 60-μm flux is probably from much a smaller mass ($<10^6\,M_\odot$) of hotter (∼200 K) dust heated by the QSO which is hidden in the case of IRAS 09104+410 (Hines & Wills 1993) or seen directly in 3C 48. Therefore the gas-to-dust ratios for these objects in Table 9 are severely underestimated as a much lower dust temperature is assumed.

The question of the origin of the observed dust is still an open one, with injection from star formation, stellar mass loss and liberation from cold clouds all plausible explanations. The spluttering time-scale owing to X-rays can be circumvented in these models through rapid generation or shielding. Given the extreme properties of cluster cores, it would be surprising if galactic gas-to-dust ratios applied in these environments.

One additional point to note with respect to the dust emission is that there are several CO-detected central cluster galaxies with relatively weak radio sources, such as e.g. A1068 and RX J0821+07. Assuming a gas-to-dust ratio of 1000 for both systems, we predict 850-μm (350 GHz) flux densities of 6 and 4 mJy respectively, compared with 1.4-GHz flux densities of 8.7 and 2.4 mJy. If one takes the radio/submillimetre spectral index, $\alpha_{1.4}^{350}$, used by Carilli & Yun (1999) then these galaxies are comparable to the ultraluminous infrared galaxies found at low redshifts ($\alpha_{1.4}^{350} = -0.2$ and -0.1 compared with -0.1 and 0.2). This may imply that most of the radio emission in these radio-weak central cluster galaxies is related to the star formation and *not* a central active nucleus. On the other hand, most of our detected targets have moderately bright radio sources (20 to 100 mJy). For these, the probable $\alpha_{1.4}^{350}$ values fall in the range -0.4 to -1.0, well below the relation for starbursts presented by Carilli & Yun (1999), so these radio-weak cases are interesting exceptions and not the norm.

5.7 Comparison with other star-forming systems

If the submillimetre properties of these line-emitting central cluster galaxies are compared with nearby starbursts, ultraluminous infrared galaxies and more distant submillimetre-selected galaxies then they appear to share a great many properties. Perhaps most importantly, the evidence from optical spectroscopy (Allen 1995; Crawford et al. 1999), in terms of the excess blue light and power of the low-ionization emission lines, points to substantial and on-going star formation ($10–100\,M_\odot\,yr^{-1}$). Therefore the cores of cooling flows are forming stars at a rate comparable to that deduced from the mass flow rate derived from X-ray observations. The possibility that more distant submillimetre and infrared-selected galaxies are in fact in cooling flows (cf. IRAS 09104+4109: Kleinmann et al. 1988; Fabian & Crawford 1995; Evans et al. 1998) should be considered in the interpretation of these galaxies. Taking IRAS 09104+4109 as a case in point, it shows strong Hα emission (Evans et al. 1998) and a strong cooling flow (Fabian & Crawford 1995) but no CO detection (Evans et al. 1998). This non-detection of CO is consistent with the correlation given in Fig. 9 as long as the Hα luminosity does not exceed $10^{42}\,erg\,s^{-1}$.

Looking to more distant submillimetre-selected galaxies, it is possible that galaxies such as 4C 41.17 (Dunlop et al. 1994) and 8C 1435+635 (Ivison et al. 1998) have more in common with central cluster galaxies than with the more commonly assumed archetypes of Arp 220 and M82. The combination of active nucleus and starburst in NGC 1275 illustrates the difficulty in classifying very

distant galaxies into 'monster' or 'starburst'. We are probably witnessing the on-going formation of a giant elliptical galaxy in these systems, and the process that is postulated to occur in the more distant galaxies. The study of these rare, low-redshift galaxies could provide important clues to the nature of distant systems.

6 CONCLUSIONS

We have, through the combination of better receivers and selection of more extreme cooling flows, succeeded in detecting molecular emission in as many as 16 central cluster galaxies. These detections are consistent with molecular gas warmed to 20–40 K by young stars. While the mass of molecular gas is 5–10 per cent of that expected to have been deposited in these cooling flows in total, it may only fill a relatively small volume of the core, so may be either on the warm tip of a cold iceberg or the sum total of the deposited mass if cooling flows are not as large as previously thought.

The commonly held view that central cluster elliptical galaxies are the oldest and most quiescent of galaxies is difficult to square with the variety of observations showing a dusty, gas-rich environment fuelling substantial star formation. The common feature amongst these peculiar galaxies is that they all lie in the cores of massive cooling flows and have relatively low radio powers. The exact mechanism that links these observations is not clear, but the association is too strong to be dismissed. This possible causal link between cooled gas and star formation is one that has substantial implications for the interpretation of distant radio- and submillimetre-selected galaxies.

The results presented in this paper indicate that observations with current and future instrumentation will be very productive. With SCUBA capable of detecting dust in the more extreme systems ($> 5 \times 10^7\,M_\odot$), and JCMT and IRAM available to detect several CO transitions and their isomers and other atomic and molecular lines such as C I, HCN, CS and H_2O, the immediate prospects are excellent. We have also recently obtained Owens Valley Radio Observatory observations of CO(1–0) for A1068, A1835, Zw 3146, RX J0338+096 and RX J0821+07, and these results will be presented separately (Edge & Frayer, in preparation). In the longer term, the development of millimetre arrays will allow the molecular gas to be spatially resolved, and missions such as SOFIA, *SIRTF* and *FIRST* offer the opportunity to sample far-infrared lines from the gas sampled by CO and any that is colder. While the ultimate fate of gas being deposited in a cooling flow is not resolved, it is encouraging to find at least some molecular gas in the cores of cooling flows.

ACKNOWLEDGMENTS

ACE thanks the Royal Society for generous support. Particular thanks go to Harald Ebeling, Andy Fabian, Carolin Crawford and Steve Allen without whom the selection of the BCS cooling flows would not have been possible. Rob Ivison, Ian Smail, Dave Frayer, Roderick Johnstone, Glenn Morris, Richard Wilman and Terry Bridges are thanked for help and encouragement. Scott Chapman is thanked for communication of SCUBA results before publication. The success of the observations presented in this paper is due largely to the excellent facilities and staff of the JCMT and IRAM telescopes. We are especially grateful to Per Frieberg, Gilles Niccolini, Gabriel Paubert and Teresa Gallego for performing the first JCMT and additional IRAM observations in service mode. Per deserves particular thanks for making the observations during the Festive Season. Finally, thanks to the referee Chris O'Dea for being far prompter and less verbose than the author. JCMT is operated by the Joint Astronomy Centre on behalf of the PPARC, the Netherlands Organization for Scientific Research and the National Research Council of Canada. This research has made use of the NASA/IPAC Extragalactic Database (NED), which is operated by the Jet Propulsion Laboratory, California Institute of Technology, under contract with the National Aeronautics and Space Administration; and the Canadian Astronomy Data Centre, which is operated by the Herzberg Institute of Astrophysics, National Research Council of Canada.

REFERENCES

Aalto S., Booth R. S., Black J. M., Johansson L. E. B., 1995, A&A, 300, 369
Allen S. W. et al., 1992, MNRAS, 257, 67
Allen S. W., 1995, MNRAS, 276, 947
Allen S. W., 1998, MNRAS, 296, 392
Allen S. W., 2000, MNRAS, 315, 269
Allen S. W., Fabian A. C., Edge A. C., Bautz M. W., Furuzawa A., Tawara Y., 1996, MNRAS, 283, 263
Allen S. W., Fabian A. C., Johnstone R. M., Arnaud K. A., Nulsen P. E. J., 2001, MNRAS, 322, 589
Antonucci R., Barvanis R., 1994, AJ, 107, 448
Braine J., Dupraz C., 1994, A&A, 283, 407
Braine J., Wyrowski F., Radford S. J. E., Henkel C., Lesch H., 1995, A&A, 293, 315
Bregman J. N., Hogg D. E., 1988, AJ, 96, 455
Bridges T. J., Irwin J. A., 1998, MNRAS, 300, 967
Carilli C., Yun M. S., 1999, ApJ, 513, L13
Carilli C., Menten K. M., Yun M. S., 1999, ApJ, 521, L25
Chapman S. C., Scott D., Borys C., Fahlman G. G., 2001, MNRAS, in press (astro-ph/0009067)
Cowie L. L., Binney J., 1977, ApJ, 215, 723
Crawford C. S., Edge A. C., Fabian A. C., Allen S. W., Böhringer H., Ebeling H., McMahon R. G., Voges W., 1995, MNRAS, 274, 75
Crawford C. S., Allen S. W., Ebeling H., Edge A. C., Fabian A. C., 1999, MNRAS, 306, 857
Deane J. R., Trentham N., 2001, MNRAS, 326, 1467
Donahue M., Mack J., Voit G. M., Sparks W., Elston R., Maloney P., 2000, ApJ, 545, 670
Dunlop J. A., Hughes D. H., Rawlings S., Eales S. A., Ward M. J., 1994, Nat, 370, 347
Ebeling H., Edge A. C., Böhringer H., Allen S. W., Crawford C. S., Fabian A. C., Voges W., Huchra J. P., 1998, MNRAS, 301, 881
Edge A. C., Fabian A. C., Allen S. W., Crawford C. S., White D. A., Böhringer H., Voges W., 1994, MNRAS, 270, L1
Edge A. C., Ivison R. J., Smail I. R., Blain A. W., Kneib J.-P., 1999, MNRAS, 306, 599
Evans A., Sanders D. B., Cutri R. M., Radford S. J. E., Surace J. A., Solomon P. M., Downes D., Kramer C., 1998, ApJ, 506, 205
Evans A., Sanders D. B., Surace J., A ., Mazzarella J. M., 1999, ApJ, 511, 730
Fabian A. C., 1994, ARA&A, 32, 277
Fabian A. C., Crawford C. S., 1995, MNRAS, 274, L63
Fabian A. C., Nulsen P. E. J., 1977, MNRAS, 180, 479
Fabian A. C., Mushotzky R. F., Nulsen P. E. J., Peterson J. R., 2001a, MNRAS, 321, L20
Fabian A. C., Sanders J. S., Ettori S., Taylor G. B., Allen S. W., Crawford C. S., Iwasawa K., Johnstone R. M., 2001b, MNRAS, 321, L33
Falcke H., Rieke M. J., Rieke G. H., Simpson C., Wilson A. S., 1998, ApJ, 494, L155
Ferland G., Fabian A. C., Johnstone R. M., 1994, MNRAS, 266, 399
Fischer J. U., Hasinger G., Schwope A. D., Brunner H., Boller T., Trumper J., Voges W., Neizvestny S., 1998, A&A, 319, 347
Fujita Y., Tosaki T., Nakamichi A., Kuno N., 2000, PASJ, 52, 235

Gear W., Robson E. I., Gee G., Nolt I. G., 1985, MNRAS, 217, 287
Grabelsky D. A., Ulmer M. P., 1990, ApJ, 355, 401
Hansen L., Jorgensen H. E., Norgaard-Nielsen H. U., 1995, A&A, 297, 13
Heckman T. M., Baum S. A., van Breugel W. J. M., McCarthy P., 1989, ApJ, 338, 48
Hines D. C., Wills B. J., 1993, ApJ, 415, 82
Holtzman J. A. et al., 1992, AJ, 103, 691
Hu E. M., Cowie L. L., Kaaret P., Jenkins E. B., York D. G., Roesler F. L., 1983, ApJ, 275, L27
Hutchings J. B., Balogh M. L., 2000, ApJ, 119, 1123
Ivison R. J. et al., 1998, ApJ, 494, 211
Iwasawa K., Allen S. W., Fabian A. C., Edge A. C., Ettori S., 1999, MNRAS, 306, 467
Jackson N., Browne I. W. A., 1991, MNRAS, 250, 414
Jaffe W., 1987, A&A, 171, 378
Jaffe W., Bremer M. N., 1997, MNRAS, 284, L1
Kleinmann S. G., Hamilton D., Keel W. C., Wynn-Williams C. G., Eales S. A., Becklin E. E., Kuntz K. D., 1988, ApJ, 328, 161
Komatsu E., Kitayama T., Suto Y., Hattori M., Kawabe R., Matsuo H., Schindler S., Yoshikawa K., 1999, ApJ, 516, L1
Lester D. F., Zink E. C., Doppmann G. W., Gaffney N. I., Harvey P. M., Smith P. M., Malkan M., 1995, ApJ, 439, 185
Lim J., Leon S., Combes F., Trung D.-V., 2001, ApJ, 549, L93
McNamara B. R., Jaffe W., 1994, A&A, 281, 673
McNamara B. R., Wise M., Sarazin C. L., Jannuzi B. T., Elston R., 1996, ApJ, 466, 66
Norgaard-Nielsen H. U., Goudfrooij P., Jorgensen H. E., Hansen L., 1993, A&A, 279, 61
O'Dea C. P., Baum S. A., Maloney P. R., Taccone L. J., Sparks W. B., 1994, ApJ, 422, 467
Owen F. N., Ledlow M. J., Keel W. C., 1995, AJ, 109, 14
Papadopoulos P. P., Seaquist E. R., 1998, ApJ, 492, 521
Papadopoulos P. P., Röttgering H. J. A., van der Werf P. P., Guilloteau S., Omont A., van Breugal W. J. M., Tilanus R. P. J., 2000, ApJ, 528, 626
Pedlar A., Ghataure H. S., Davies R. D., Harrison B. A., Perley R., Crane P. C., Unger S. W., 1990, MNRAS, 246, 477
Peres C. B., Fabian A. C., Edge A. C., Allen S. W., Johnstone R. M., White D. A., 1998, MNRAS, 298, 416
Perlman E. S., Padovani P., Giommi P., Sambruna R., Jones L. R., Tzioumis A., Reynolds J., 1998, AJ, 115, 1253
Peterson J. R. et al., 2001, A&A, 365, L104
Pinkney J. et al., 1996, ApJ, 468, L13
Romanishin W., Hintzen P., 1988, ApJ, 324, L17
Sahu K. C. et al., 1998, ApJ, 492, L125
Sanders D. B., Scoville N. Z., Soifer B. T., 1991, ApJ, 370, 158
Schindler S. et al., 1995, A&A, 299, L9
Soker N., White R. E., III, David L. P., McNamara B. R., 2001, ApJ, 549, 832
Solomon P. M., Downes D., Radford S. J. E., Barrett J. W., 1997, ApJ, 478, 144
Tamura T. et al., 2001, A&A, 365, L87
Van den Bergh S., 1977, Astron. Nachr., 298, 285
Voit G. M., Donahue M., 1995, ApJ, 452, 164
White D. A., Fabian A. C., Johnstone R. M., Mushotzky R. F., Arnaud K., 1991, MNRAS, 252, 72
White D. A., Jones C., Forman W., 1997, MNRAS, 292, 419
Wilman R. J., Edge A. C., Johnstone R. M., Crawford C. S., Fabian A. C., 2000, MNRAS, 318, 1232
Wilman R. J., Edge A. C., Johnstone R. M., Fabian A. C., Allen S. W., Crawford C. S., 2001, MNRAS, submitted
Young J. S., Sanders D. B., 1986, ApJ, 302, 680
Zepf S. E., Carter D., Sharples R. M., Ashman K., 1995, ApJ, 445, L19

This paper has been typeset from a TEX/LATEX file prepared by the author.